Trajectory Simulation of fast ions in Tokamak

by

Abdullah

Submitted to the Department of Physics
in partial fulfillment of the requirements for the degree of

Master of Philosophy

at the

QUAID-I-AZAM UNIVERSITY

June 2014

Signature of Author .....
Department of Physics
25 June 2014

Certified by .....
Dr. Majid Khan
Assistant Professor
Thesis Supervisor

Accepted by .....
Dr. Arshad Majeed Mirza (S.I)

Trajectory Simulation of fast ions in Tokamak

by

Abdullah

Submitted to the Department of Physics
on 25 June 2014, in partial fulfillment of the
requirements for the degree of
Master of Philosophy

Abstract

A numerical scheme based on Symplectic Integration Algorithm (SIA) has been used to calculate fast ion trajectories in tokamak magnetic configuration. First the superiority of the symplectic algorithm over the non symplectic algorithm, like Range-Kutta Algorithm (RKA), has been demonstrated by solving a simple problem namely the Henon-Heiles Hamiltonian. In this regard the stability of the schemes as well as the energy conservation in long period calculations have been highlighted. The phase space trajectories of stars were investigated for different initial conditions and different energies and it is concluded, for long time simulations, the energy of a given star is well conserved in case of SIA while in case of RKA energy is not conserved therefore for long time simulations SIA is of great importance and is impossible to ignore it.

Then SIA has been used to find the exact trajectories of, trapped and passing, fast ions in tokamak (fusion reactor) toroidal devices. In particular, we have investigate the effect of an intrinsic magnetic field perturbation, i.e. toroidal field ripples which are there due the discrete number to toroidal coils around the torus. The simulations are carried out for circular flux surfaces. Again we have found that the numerical scheme used shows excellent conservations of particle energy as well as angular momentum (in axi-symmetric fields). The effect of TF-ripples on these trajectories has been investigated and it is shown that the resonance between toroidal precession of bananas and the toroidal field ripples can result in spreading of the trajectories meaning thereby that an enhanced radial diffusion of fast ions.

Thesis Supervisor: Dr. Majid Khan
Title: Assistant Professor

Contents

1 Introduction **5**

2 Review of charged particle motion in electromagnetic field **11**

2.1 Single particle description 11

2.1.1 Guiding center motion 12

2.1.2 Adiabatic Invariants 13

2.1.3 Particle orbits in tokamak 15

2.2 Hamiltonian formalism and derivation of canonical coordinates 22

2.2.1 Magnetic fields and magnetic fluxes 23

2.2.2 Lagrangian of guiding center motion 24

2.2.3 Canonical coordinates 31

3 Method of Symplectic integration **35**

3.1 Integration of Hamiltonian System 35

3.2 Symplectic integration of a general Hamiltonian system 37

3.3 Application of SIA to Henon-Heiles Hamiltonian : *Motion of stars about a galactic center* 41

3.3.1 Comparison of SIA and RKA 42

3.3.2 Sensitivity of SIA and RKA 46

4 Trajectory calculation of fast ions in tokamak using SIA **51**

4.1 Model for steady-state magnetic field perturbations 51

4.1.1 Model for safety factor q_s and poloidal flux ψ 52
4.1.2 Model for TF ripples perturbation b_{TFR} 54
4.1.3 Super banana orbits and ripples resonances 55
4.2 Trajectories of fast alpha particles in tokamak in axi-symmetric B-field 56
4.3 Alphas trajectories in the presence of TF-ripples 62
4.4 Conclusion 65

Chapter 1

Introduction

The increasing demand of energy is the result of growing population and speedy urbanization. In this regard there are two main problems: the increasing need of energy and the limited sources of energy. The solution to these problems is the usage of energy in a more effective way and development of new technologies. The current energy supply mix has some serious disadvantages. For example in the sense that about 81% of the total energy is deduced from fossil fuels, such as coal, oil and natural gas supplies [1]. From the use of fossil fuels, world faces different problems, such as pollution due to mining and burning, limited reserves and unequal distribution around the earth due to which great struggle is needed to get access to these reserves. One big problem which affects all mankind is the production of CO_2 from burning of fossil fuels [2].

Sources other than fossil fuels are hydro (currently 2.2% of world energy production), combustible renewables or biomass (9.8%, of which a large fraction is traditional (wood fires) and waste combustion), energy sources having strong growth potential are solar and wind energy sources (currently 0.7%) [1]. However its very difficult for solar energy and wind energy to completely replace the fossil fuel. Since renewables such as solar and wind require large areas of land and sea so thereby prevent other use of land such as agriculture, moreover their efficiency is not too high and it may take many decades before these sources generate a reasonable share of the energy mix.

Another most important source of energy is nuclear energy in which energy is produced through nuclear reactions, i.e. splitting of heavy atom into light atoms. Such nuclear reactions are called fission reactions. Now a days 5.9% of the world total energy is provided by nuclear fission, i.e. mostly from the Uranium isotopes splitting. However, Uranium is available only in limited amount on the surface of earth.

The proposed solution to such problems is the "Nuclear Fusion energy " also called an "endgame" source of sustainable energy. The reaction in which two or more than two light atomic nuclei collide to each other at a very high speed and join to form a new heavy atomic nuclei with the production of large amount energy is called nuclear fusion reaction. Matter is not conserved in nuclear fusion process because during nuclei fusing some of mass is converted into energy. Advantages of nuclear fusion can be summarize as follow:

- It is unclouded, i.e. it do not expel any greenhouse gases. Also it is Co_2 free.
- It is risk-free, i.e. materials like tritium in fusion reactor is radio-active but all these have half life is much less, than those in nuclear fission, and it decays to a secure level. Most importantly, in contrast to the fission reaction, no chain reactions are involved in a fusion reactions.
- Fuel used in fusion reactions are easily available, e.g. for a DT reaction (which is the most probable reaction among other possibilities). Deuterium is naturally abundant (0.015% of all water) and fuel like tritium can be obtained from lithium, e.g.

$$\mathrm{Li}^6 + n^1 \rightarrow \mathrm{T}^3 + \mathrm{He}^4$$

$$\mathrm{Li}^7 + n^1 \rightarrow \mathrm{T}^3 + \mathrm{He}^4 + n^1$$

However, one of the most important and basic problem associated with nuclear fusion is that it is much challenging to achieve, hundreds of millions kelvin temperature needed to burn the fuel required for thermonuclear fusion. This is because of the following reason: to get the nuclei to come close enough and prevail over the Coulomb's repulsive force, between two positive charged nuclei, they need to collide with a very high speed. This means that the particles need to have a very high temperature: in a fusion reactor the temperature is millions of degrees and the fuel is in the plasma state.

Different experimental arrangement have been done to attain a specific energy gain from fusion by using various confinement concepts. For example the inertial confinement fusion in which a power full laser pulse is used for fusion fuel compression. The next type of confinement is magnetic confinement in which magnetic field is used for confinement of fusion fuel [3].

Sun and all other stars are providing large amount of energy through inertial confinement which is due to large inertia (mass) of sun and all other stars. In a single moment it pumps out such a huge amount of energy that it is million times greater than used by the total people in universe in a year [3].

Fusion research is and always has been an international enterprise. Since the 1955 *Atoms for Peace Conference* held in Geneva fusion scientists from all over the world have freely exchanged ideas and visited international conferences. Currently, European Union, Russian Federation, China, USA, South korea, Japan and India are working to build the next generation fusion experiment, ITER, which stands for International Thermonuclear Experimental Reactor. This world in Latin mean "journey", "way" or "direction" all these words show the potential of ITER ruling nuclear fusion as a source of peaceful energy. The motto of building this machine is "The way to new energy". ITER is consider as the biggest project ever in the world, it is expected that it will overcome all energy shortage problems and will benefit all mankind. The ratio of output power (fusion power) to input power for ITER which is represented by a symbol Q is: $Q \geq 10$ which indicates that ITER output power production will be 10 times greater than its input consumption. ITER is designed for the production of 500 MW fusion power. Isotopes of hydrogen like Deuterium and Tritium are expected to be used as a fuel. To convert it to hot plasma state, temperature of fuel in ITER will be raised upto 150 million $^{\circ}C$.

Nuclear fusion works on very simple rules: decrease in total mass occur when two light nuclei such that deuteron (D^+) and triton (T^+) or two deuterons under some specific reaction conditions combine together and as a result some energy is produced in the form of kinetic energy. Some of nuclear fusion reactions are

$$D^2 + D^2 \rightarrow T^3 + H^1 + 4.1 \text{ MeV}$$
$$D^2 + D^2 \rightarrow He^3 + n^1 + 3.2 \text{ MeV}$$
$$D^2 + T^3 \rightarrow He^4 + n^1 + 17.6 \text{ MeV}$$
$$D^2 + He^3 \rightarrow He^4 + H^1 + 18.3 \text{ MeV}$$

$T^3 + T^3 \rightarrow 2n^1 + He^4 + 11.3$ MeV

$T^3 + He^3 \rightarrow H^1 + He^4 + n^1 + 12.1$ MeV

$He^3 + He^3 \rightarrow 2H^1 + He^4 + 12.9$ MeV

However, the basic disadvantage of nuclear fusion is confinement. Confinement of fuel and high energetic charged particles, e.g. produced in the fusion reaction as a product, which can give their extra energy to plasma species and required temperature to maintain nuclear fusion reaction.

Different techniques are used to confine the plasma to reaction volume at some specific temperature. Here we are going to discuss one of the advance concept of a fusion reactor, namely, tokamak which works on magnetic confinement concept [4], where magnetic fields are used to control the orbit motion of plasma elements, i.e. electrons and ions. The word tokamak comes from Russian language and is composition of "toroidal'naya kamera s magnitnymi katushkami" means a toroidal chamber with magnetic coils used for toroidal confinement. Tokamak was developed by Soviet plasma physicists in 1960s.

Nuclear fusion is impossible until the plasma is heated to a certain temperature to provide specific heat energy to plasma. It is far important to confine the fast energetic ions, produced by neutral beam injection (NBI), by radio frequency (RF) heating and in fusion reactions, in the center of tokamak plasma. The fast ions like Helium ions which are produced in fusion reactions as a product have an identical arrangement of velocity vector at 3.5 MeV. While fast ions produced through NBI and ICRH (ion cyclotron resonance heating) have only specific direction velocity vectors. Those fast ions whose velocities are perpendicular to $\mathbf{B}$ are generated by ICRH process. ICRH process is that process in which plasma ions are accelerated through electromagnetic waves to specific limit of several hundreds keV at their gyro frequency. In NBI (the process in which plasma heating occur through injection of neutral beams) system the velocity vector depends on Neutral beam injection geometry and its acceleration. As neutral particles are not effected by electric and magnetic fields, in analogue to that NBI also can not be effected by electric and magnetic fields of tokamak. Hence to achieve convenient plasma burning condition fast ions play a very critical role. Losses of energetic ions from tokamak plasma occur through different mechanisms, e.g. first orbit losses, by scattering, by collective plasma instabilities and by diffusive transport mechanisms etc. [5, 6].

The lost fraction of fast ions can be evaluated using kinetic approach by calculating the transport coefficients among which coefficient for radial diffusion (perpendicular to the so-called flux surfaces in which the magnetic field lines lie) is a crucial one for confinement judgment. For the accurate calculations of radial diffusion, the exact knowledge of particle trajectories is required. A method based on numerics is required to find the trajectories from which one can find transport coefficients of fast ion for tokamak plasma under the influence of magnetic field having periodic, in space and time, perturbations.

The numerical method used here is called the Symplectic Integration Algorithm (SIA), it is a type of numerical method in which errors are not collected at each step of time, even do not produce large numerical dispersion by the iteration routine. This is due to satisfying specific condition known as *symplectic* condition at each integration step [7]. Hence it demonstrate the preservation of the canonical structure of the equation of motion in the frame-work of Hamilton's equations. By using same integration step size and same order of accuracy it has been observed that trajectory calculated in the result of symplectic method has greater accuracy as compere to trajectory in the result of non-symplectic method for same initial conditions [8, 9, 10, 11]. The accuracy results in the symplectic method is due to energy and momentum conservation upto great extant. SIA is also efficient for those dynamical systems which needs long time scale assessment and having large size integration step this is due to the fact that small variation occur in energy. Due to same reason its good to use SIAs, for trajectory simulation of fast ions in tokamaks for large time scales [10, 12].

For interpreting and predicting the behavior of energetic ions in present and,respectively, future fusion tokamaks like ITER, it is important to examine and understand fast ion transport in the presence of perturbations of the confining magnetic field [13, 14, 15]. As a result of theoretical and experimental observation it is clear that alpha particles produced by axisymmetric magnetic field model of high-current tokamak DT reactor are easy to confine and play a pivot role to heat the tokamak plasma (self-heating effect) to fusion temperature [16, 17]. However, certain perturbations disturbs fast ion transport such as Toroidal field (TF) ripples and magnetohydrodynamics (MHD) modes. These perturbations can cause fast ion loss from tokamak [15, 18]. Our work in this dissertation focus on this issue.

In the outer region of plasma or region near the outer wall of tokamak TF ripples are very

frequent and has the power to diffuse fast ions very quickly. For example theory and simulations both indicates that through some MHD process if a low quantity (less than 10 %) of fast ions is shifted from core of plasma to the outer edge and hence increase radial transport of fast ions, and these fast ions which through diffusion move from central part of plasma to the outer edge damage the outer wall of fusion reactor tokamak [19, 20].

SIA can be used to study the effects of different perturbations like TF ripples on trajectory of fast ion. Manifestation of SIA become so simple if we are dealing with circular flux surfaces (FS), so to perform the task easily we suppose tokamak magnetic configuration with circular flux surfaces.

Here the main goal of this work is to focus our attention on the trajectory calculation of those fast alpha particles which are toroidally trapped in non homogenous axisymmetric magnetic field of tokamak, due to which bouncing phenomena occur between higher field strengths. These fast alpha particles traces out a special shape orbit which look like banana when viewed poloidally and hence these are refer to as banana orbits. Through resonance phenomena TF ripples mostly affect trapped alpha particles and can increase radial diffusion of energetic ions. Resonance also produce another type of orbit called superbanana orbit [21] which is shaped due to guiding center motion of banana orbits such orbit is obtained when resonance occur between bounce motion and periodic manner of TF ripples. The required resonance condition is

$$N\omega_t = l\omega_b,$$

where N describes the number of loops (coils) which produce toroidal field, ω_t refers for frequency of toroidal precession, ω_b represents bounce frequency and l corresponds to a rational number, the most important point about l to remember is that resonance occur when l has value of integer or its integral multiple. After justification of resonance condition, a frequent extension occur in collisional radial displacement under the influence of periodic perturbation in TF ripples and due to this reason fast ions losses starts from confined region. A numerical model depends on orbit following symplectic simulations has been designed which can further be used to find collisional fast ion diffusion due to TF ripples and resonance phenomena [18].

Chapter 2

Review of charged particle motion in electromagnetic field

2.1 Single particle description

Electric and magnetic forces restricts the motion of plasma charge particles in magnetic confinement fusion (MCF) process, whereas no affect occur in electric and magnetic fields due to this motion. Strictly speaking a minor change occur in the fields due to each particle motion but the change is so small and is ignored. For a non-relativistic charged particle i, having mass m_i and charge q_i, the fundamental equation of motion is

$$m_i \frac{dv_i}{dt} = q_i \left(E + v_i \times B\right) + F_i^{ext}, \tag{2.1}$$

where F_i^{ext} refers to some external forces effecting charge particle motion such as gravitational forces which play a key role in astro-plasmas. Therefore while writing its equation of motion it is important to replace F_i^{ext} by a gravitational force term, whereas in MCF devices like tokamak and stellarators, gravitational force is very small as compare to magnetic and electric forces and is neglected. Magnetic force has the property to cause circulation of charge particles around its field lines (gyration), so it is clear from Lorentz force, i.e. $q_i \left(v_i \times B\right)$ that if a component of velocity parallel to magnetic field is present then it will enforce the charge particle to gyrate it. But the system here is tokamak, having toroidal configuration, in which

magnetic field lines are not straight (curved) and also the field is not a uniform one due to these two factors separation of charge phenomena come in to action and these separation of charges produce an extra electric field in the whole system. So an extremely large magnetic field is needed to confine a hot thermonuclear fusion plasma. For those machines which works on MCF concept, all kind of forces is dominated by Lorentz-forces.

2.1.1 Guiding center motion

Practically it is very difficult to accurately integrate the equation of motion for those **E** and **B** which depends on time and space. As charge particle revolve and move around the field lines, in the presence of electric and magnetic forces, by taking average of entire rotations we get center of gyration also known as guiding center. The equations becomes lot easier and can be handled by our numerical tools. Hence we ignore the fast gyro-motion and follow the guiding center motion. As mentioned that the system used here is tokamak a MCF-machine in which the field lines are not straight but are curved, moreover **B** is not uniform, charge separation produce electric field all these factors is a source to produce motion of guiding center perpendicular to magnetic field. Velocity of guiding center can be written as [5].

$$\mathbf{v}_{gc} = v_{\parallel}\hat{b} + \frac{\mathbf{E}\times\mathbf{B}}{B^2} + \frac{v_{\parallel}^2\hat{b}\times\left(\hat{b}\cdot\nabla\right)\hat{b} + \mu\hat{b}\times\nabla B}{\omega_g}, \tag{2.2}$$

where $\hat{b} = \mathbf{B}/B$, magnetic field strength is represented by B, ω_g denotes charge particle circulating frequency, which can be written as $\omega_g = Ze\mathbf{B}/m$ where m gives mass of particle, e denotes electron charge, Z is particle charge state, magnetic moment is represented by $\mu = mv_{\perp}^2/2\mathbf{B}$, particle velocity components $\parallel$ (parallel) and $\perp$ (perpendicular) to magnetic field are $v_{\parallel}$ and $v_{\perp}$, respectively. The 1^{st} term in Eq. (2.2) indicates motion of guiding center along the field lines when guiding center having its $\parallel$ component of velocity, second part of Eq. indicate the $\mathbf{E}\times\mathbf{B}$ drift across field lines, this drift does not depend on plasma particle mass, charge and velocity and hence equally affect all plasma particles. The last term of equation represents the combine effect of both curvature drifts and ∇B drift; each of these drifts depends on plasma particles mass and charge and due to these drifts a phenomena known as charge separation occur i.e. electrons and ions move away from each other. When particles move along curved

field lines centripetal acceleration is produced, this centripetal acceleration is responsible for the production of curvature drift (perpendicular to both **B** and curvature vector). Gyro radius, ρ_g, is large for weaker B and vice versa. If gradient of magnetic field is at 90° to magnetic field, then it results in a type of drift known as grad-B drift, $\perp$ to both **B** and gradient of magnetic field, ∇B.

Charge particle trace out a specific trajectory when it move in electric and magnetic field to find this trajectory accurately, the better option is to use guiding center drift motion method. The method used is much affective in the case when changes occur very slowly in space and time, i.e. when ρ_g is very small as compare to any scale length for a non homogenous field and frequency of gyration, ω_g is a lot greater as compare to any other field frequency [22].

2.1.2 Adiabatic Invariants

From Ref. [5] we can define a quantity which does no change when the particle move in a slowly varying fields under some specific low order approximation is called an adiabatic invariant. Adiabatic invariance is acceptable only for a very small and slow changing fields (electric and magnetic), which are responsible for the trajectory of moving particle. The word small convey the message that time variation of fields will be such that the gyro period will be smaller than it, i.e. particle frequency of gyration ω_g is a lot greater as compare to any other field frequency. Finally, in case of adiabatic invariance the space changes occur in field is related to length scale which is more longer than Larmor radius ρ_g.

Magnetic Moment

Circular motion of charge particle across the magnetic field lines results in a current represented by symbol I_c. For circular current loop the magnetic moment is defined as

$$\mu = I_c A, \tag{2.3}$$

where $I_c = Ze\omega_g/2\pi$, with $\omega_g = ZeB/m$, and A represents area of circular orbit, i.e.

$A = \pi\rho_g^2$, by putting values of I_c, ω_g and A in Eq. (2.3) we find

$$\mu = \frac{\frac{1}{2}mv_\perp^2}{B} \tag{2.4}$$

Magnetic moment depending on smallness of magnetic filed variations is an adiabatic invariant. The average force can be written as [23]

$$F_z = -\frac{1}{2}\frac{mv_\perp^2}{B}\frac{\partial \mathbf{B}}{\partial Z} \tag{2.5}$$

$$F_z = -\mu\left(\frac{\partial \mathbf{B}}{\partial Z}\right) \tag{2.6}$$

In general form this force become

$$F_\parallel = -\mu\frac{\partial \mathbf{B}}{\partial s} = -\mu\nabla_\parallel \mathbf{B} \tag{2.7}$$

where ds gives line element along magnetic field. Larmor radius is strongly affected by the change in magnetic field strength while magnetic moment show no such dependence and will remain invariant. Consider those component of equation of motion which are parallel to magnetic field

$$m\frac{dv_\parallel}{dt} = -\mu\frac{\partial \mathbf{B}}{\partial s} \tag{2.8}$$

Multiply left side by $v_\parallel$ and right side by ds/dt. We find

$$mv_\parallel\frac{dv_\parallel}{dt} = -\mu\frac{\partial \mathbf{B}}{\partial s}\frac{ds}{dt} \tag{2.9}$$

$$\frac{d}{dt}\left(\frac{1}{2}mv_\parallel^2\right) = -\mu\frac{d\mathbf{B}}{dt} \tag{2.10}$$

$d\mathbf{B}/dt$ shows change in magnetic field with time. According to law of conservation of energy we have

$$\frac{d}{dt}\left(\frac{1}{2}mv_{\parallel}^{2}+\frac{1}{2}mv_{\perp}^{2}\right)=\frac{d}{dt}\left(\frac{1}{2}mv_{\parallel}^{2}+\mu\mathbf{B}\right)=0 \tag{2.11}$$

From the above equation

$$\frac{d}{dt}\frac{1}{2}mv_{\parallel}^{2}=-\frac{d}{dt}\left(\mu\mathbf{B}\right) \tag{2.12}$$

Put Eq. (2.12) in Eq. (2.10) we find

$$-\frac{d}{dt}\left(\mu\mathbf{B}\right)=-\mu\frac{d\mathbf{B}}{dt}$$

$$\frac{d\mu}{dt}=0 \tag{2.13}$$

In plasmas confinement (magnetic mirror), magnetic moment invariance is of key importance. $v_{\perp}$ increases when the particles move from the week magnetic field region to strong magnetic field region and hence $\mathbf{B}$ also increases which keeps magnetic moment constant.

Second adiabatic invariant also known as longitudinal invariant acts in to play only for those charge particles which has large scale periodic motion, it is represented by J_l and can be mathematically written as

$$J_l=\oint v_{\parallel}\hat{b}\cdot dx\ . \tag{2.14}$$

Integral used in the above equation indicates that it followed out full periodic orbit $x(t)$. The large scale periodic motion as mentioned above produce a specific kind of drift due to which a huge change occur in particle trajectory [5].

2.1.3 Particle orbits in tokamak

In fusion reactor like tokamak the magnetic field is not uniform and results in different type of drifts that effects particle motion. Now in this section we are going to explain trajectories of charged particles when various drifts influence on its guiding center. Toroidal and poloidal directions as well as toroidal coordinates are shown in the Fig. 2.1

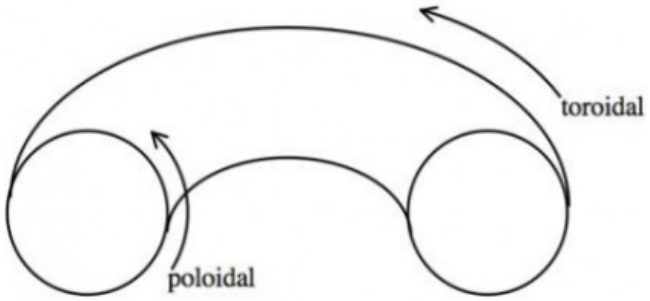

(a)

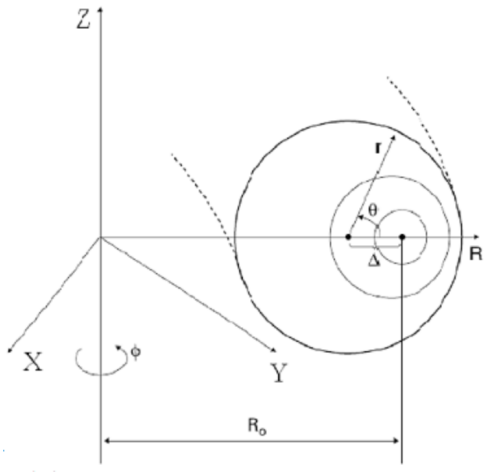

(b)

Figure 2.1: *(a) Toroidal and Poloidal directions; (b) Toroidal coordinates (r,θ, ϕ), and Cartesian coordinates (X,Y,Z)*

In Fig 2.1(b) R_o represents tokamak major radius while r shows minor radius. According to Fig 2.1(b) the cartesian coordinates and toroidal coordinates are correlated with one another as follow

$$X = R\cos\phi, \quad Y = R\sin\phi, \text{ and } Z = r\sin\theta, \tag{2.15}$$

where

$$R = R_o + r\cos\theta - \Delta(r) \tag{2.16}$$

with $\Delta(r)$ denoting the so called Shafranov shift.

First of all we suppose that only toroidal magnetic field $\mathbf{B}_t$ is there in tokamak and want to study its effect on plasma species. Tokamak has a shape of torus therefore the magnetic field present is not straight but a curve, and hence provide base for curvature drift, secondly the field we supposed is not a uniform and clearly means that grad-$\mathbf{B}$ drift will be produced. Both these drifts play their role, results in the separation of plasma charges, i.e. separation of electron and ion occur, due to separation of charges an Electric field $\mathbf{E}$, will set-up in vertical direction. Note that both electrons and ions have opposite charges and are compelled to move in opposite direction, i.e. electrons and ions move to opposite halves of the tokamak. Next important drift which is arised due to this $\mathbf{E} \times \mathbf{B}$ drift which enforce both ions and electrons to move out ward, i.e. towards the outer wall of the tokamak as depicted in Fig. 2.2.

The out flow of plasma species caused by $\mathbf{E} \times \mathbf{B}$ drift and hence we conclude that charge separation got some disadvantages i.e. it play a negative role considering confinement point of view, secondly it can result in damage the outer wall of the tokamak when these hot plasma particles strikes with it. So the main issue is to stop this out word flow of charge particles, to resolve this problem an extra magnetic field is required which helps alot to stop the charge particle out word flow. Field generally uses in such case is poloidal magnetic field $\mathbf{B}_p$. A twist is generated in magnetic field lines after applying poloidal magnetic field, the twisted $(\mathbf{B}_T + \mathbf{B}_p)$ field lines compels each plasma particle to move across these twisted field lines and in result cover whole poloidal cross section, it clearly indicate that during such twisted motion ever particle of plasma stay for same interval of time in each half of tokamak and hence also reduce charge separation effect.

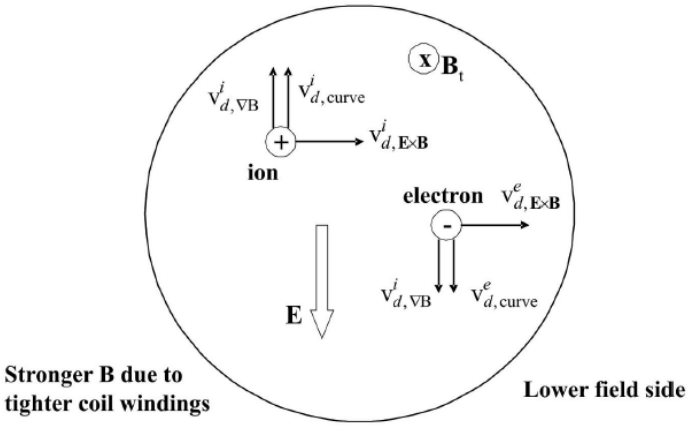

Figure 2.2: *Pure toroidal magnetic arrangement produce guiding center drifts and results in an outward drift for both ions and electrons.*

There are two categories of charge particles when it move in a device having toroidal magnetic field arrangements, passing particles: which move around the tokamak and trapped particles: which are trapped in magnetic well, magnetic well arises due to magnetic field difference at the inboard and outboard of tokamak.

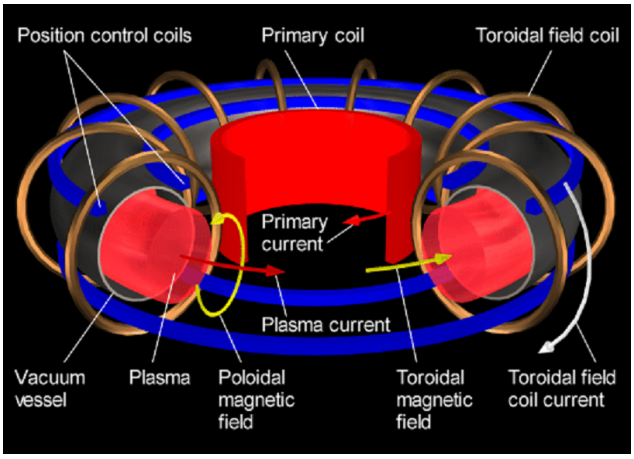

Figure 2.3: *Schematic diagram of Tokamak*

Toroidal magnetic field $\mathbf{B}_T$ is produced by the poloidal windings around the torus, it is clear that on the inner side the winding is close to each other and hence resulting in a strong magnetic field on the inner side while on the outer side of the torus the winding is away from

each other so magnetic field is weaker in the outer side. This difference of magnetic field on the sides of torus become as magnetic mirror and can trap plasma particles bearing low component of velocity parallel to **B**. Thus those charge particles whose parallel component of velocity $v_{\|}$ is less than some specific value (threshold value) indicate by larger and smaller values of magnetic field strength in torus arrangement can be trapped in magnetic mirror such particles are called trapped particles. In tokamak the friction of trapped particles are [4, 5]

$$f_{traf} \approx \sqrt{\frac{2\epsilon}{1+\epsilon}}, \tag{2.17}$$

where $\epsilon = a/R_0$ express ratio between minor radius (a) and major radius (R_0) of tokamak and is known as inverse aspect ratio. Note that almost 70% of plasma particles will be trapped for tokamak having $\epsilon \approx 1/3$. In tokamak drifts like grad-**B** and curvature drift effects all plasma particles, the plasma trapped particles move to and fro in between mirror points and in poloidal projection shaped out a trajectory known as banana orbit with a finite width Δr as shown in the Fig. 2.4 and Fig. 2.5. For circular flux surfaces, charge particles having high parallel component of guiding center velocity then it is hard for mirror points to confine such particle, the particle move on the circular trajectory around the torus and is known as passing particle. Two types of passing particles are there differentiate from each other by their motion direction, i.e. some passing particles move in the direction (co-circulation) of magnetic field lines while other move opposite to the direction (counter-circulation) to magnetic field lines. Orbit shift also occur under the influence of curvature and grad-**B**, i.e. orbit shift in inward direction for co-circulating plasma particles and orbit shift in outward direction for counter-circulating plasma particles.

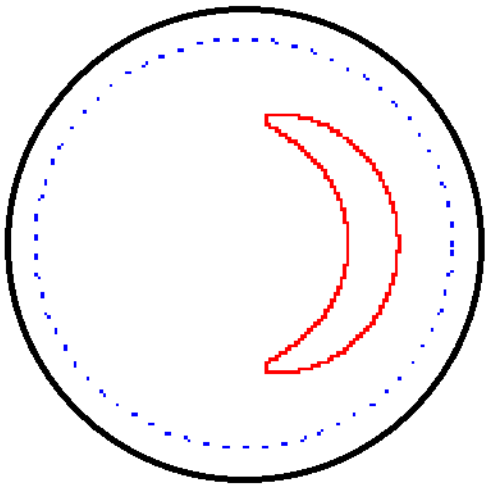

(a)

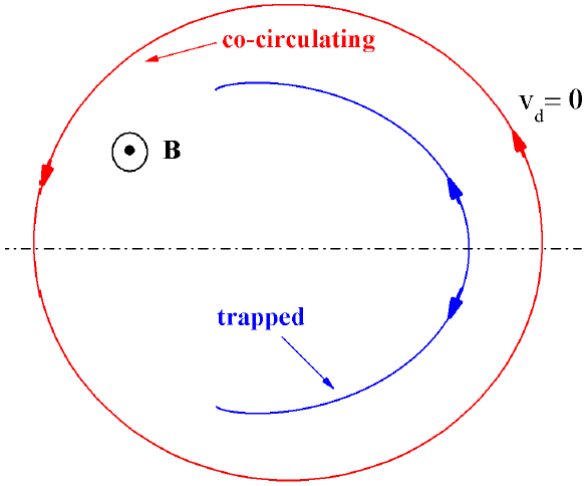

(b)

Figure 2.4: *Poloidal projections of charged particle orbits in tokamak: (a) gyro-orbital drift motion of circulating and trapped particles; (b) guiding center orbits of a counter-going (circulating) positive ions and of a trapped positive ions in the absence of drifts.*

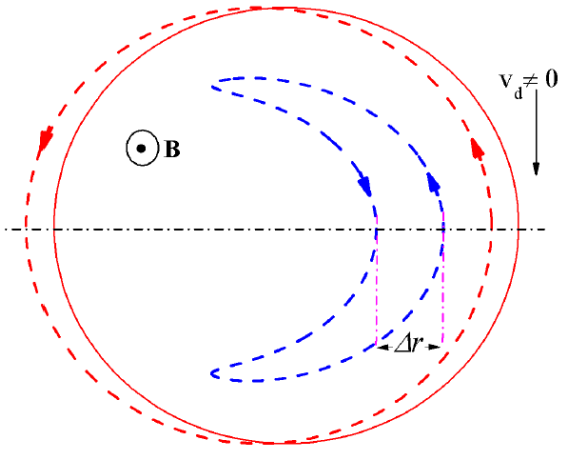

Figure 2.5: *Poloidal projections of charged particle orbits in tokamak: guiding center orbits of a counter-going (circulating) positive ions and of a trapped positive ions in the presence of a drift.*

Collisions can displace the particles from one magnetic surface to another. The maximum displacement cover by passing particles is due to collisions is up to order of gyro radius, ρ_g. While the maximum allowed distance for untrapped particles, which it cover due to collision is as that of, Δr. The resistive diffusion coefficient perpendicular to $\mathbf{B}$ is proportional to both $(\rho_g)^2$ for passing particles and $(\Delta r)^2$ for trapped particles.

The limited number poloidal coils, which produce toroidal magnetic field disturb the axisymmetry of fusion reactor tokamak. The position of these poloidal coils produce alterations in the strength of toroidal magnetic field which are term as ripples as shown in the Fig. 2.6

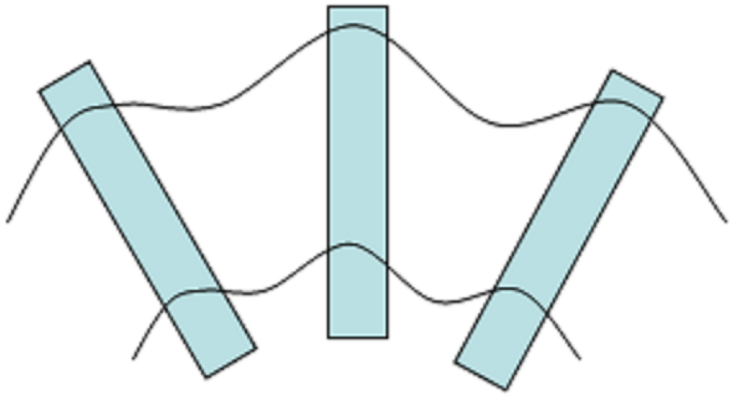

Figure 2.6: *Torodial field ripples, it shows that when we are close to the TF coils field is stronger and as you move away from them filed get weaker, i.e. ripples in TF.*

Transport mechanisms related with toroidal field ripples are of two types:

1) Ripple well trapping

2) Banana drift transport

The detail description of these phenomena is out of the scope of this work.

Toroidal field ripples produce magnetic perturbation, these magnetic perturbation greatly effects those trapped particles which are at the tips of banana orbits. These particles having $v_{\|} = 0$ at the tips [5].

2.2 Hamiltonian formalism and derivation of canonical coordinates

Drift Hamiltonian equations for fast ions can be solve through our code which is refer as SIDOC which stands for "Symplectic Integration Drift Orbit Code", here our main goal is to derive drift Hamiltonian for fast ions in tokamak. In this study the drift Hamiltonian and equation of motion for fast ions in tokamak depends on canonical coordinates, and in this section we are to going to discuss in detail set of canonical coordinates.

2.2.1 Magnetic fields and magnetic fluxes

Magnetic field can be represented in various ways. Here most general form of magnetic field used is

$$\mathbf{B} = g\nabla\zeta + I\nabla\theta + k\nabla\text{Ŧ} \tag{2.18}$$

where $\nabla\zeta$, $\nabla\theta$ and ∇Ŧ represents unit vectors. An alternate form of the magnetic field can also be written as [24]

$$\mathbf{B} = \nabla\Phi \times \nabla\theta - \nabla\zeta \times \nabla\psi,$$

$$\mathbf{B} = \nabla \times (\Phi\nabla\theta - \psi\nabla\zeta) \tag{2.19}$$

$$\mathbf{B} = \nabla \times \mathbf{A} \tag{2.20}$$

By comparing Eq. (2.19) with $\mathbf{B} = \nabla \times \mathbf{A}$, we can write the vector potential $\mathbf{A}$ in the form

$$\mathbf{A} = \Phi\nabla\theta - \psi\nabla\zeta \tag{2.21}$$

In Eq. (2.18) Ŧ represents flux surface, and is define as, any surface having two dimensions represented by any general function say Ŧ = constant, is termed as magnetic flux surface. If at any instant magnetic field lines present in the surface, i.e. $\mathbf{B} \cdot \nabla\text{Ŧ} = 0$. These type of surfaces are very important for long-term confinement through tokamak. θ define general poloidal coordinates and ζ represents general toroidal coordinates.

There are two ways to represent any vector, e.g. $\vec{A} = A_\alpha e^\alpha$ and $\overrightarrow{A} = A^\alpha e_\alpha$, and are known as covariant and contravariant components. Symbols with indices below are called covariant components, while symbols with above indices are known as contravariant components. Hence g, I and k in Eq. (2.18) defines convariant component of $\mathbf{B}$. For flux surface, $\mathbf{B} \cdot \nabla\text{Ŧ} = 0$. Hence we can write $\mathbf{B}$ in term of two other vectors perpendicular to is ∇Ŧ.

$$\mathbf{B} = B^{\theta} e_{\theta} + B^{\zeta} e_{\zeta} = J B^{\theta} \nabla\zeta \times \nabla\mathbf{F} + J B^{\zeta} \nabla\mathbf{F} \times \nabla\theta, \tag{2.22}$$

where J represent Jacobian and is written as $J^{-1} = \nabla\mathbf{F} \cdot (\nabla\theta \times \nabla\zeta)$.

2.2.2 Lagrangian of guiding center motion

In the presence of electric and magnetic fields, Lagrangian for charge particle motion is written as [25]

$$L = [A(x,t) + v] \cdot \dot{x} - H(v,x), \tag{2.23}$$

where H represents Hamiltonian, x position and v velocity. Conventionally m_i and e_i which is mass and charge of particles, respectively, are taken as 1 [24, 26]. Classify velocity into its parallel and perpendicular components with respect of $\mathbf{B}$, as

$$v = v_{\parallel} + v_{\perp} = v_{\parallel}\hat{b} + v_{\perp}\hat{c} \tag{2.24}$$

Here $\hat{b} = \mathbf{B}/B$ and $\hat{c} = -\sin\xi\hat{e}_1 - \cos\xi\hat{e}_2$, with ξ indicating gyro-phase, $\hat{e}_1$ and $\hat{e}_2$ indicates unit vectors perpendicular to magnetic field, i.e. $\hat{e}_1 \times \hat{e}_2 = \hat{b}$. Particles guiding canter is define by the relation

$$x = X + \frac{v_{\perp}}{B}\hat{a} \tag{2.25}$$

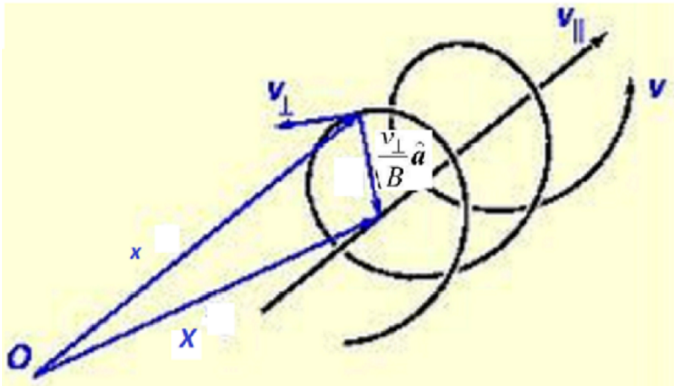

Fig. 2.7: *Any point on the particle trajectory can be represented in term of guiding center coordinates.*

By taking time derivative of Eq. (2.25), we have

$$\dot{x} = \dot{X} + \frac{d}{dt}\left(\frac{v_\perp}{B}\hat{a}\right) \tag{2.26}$$

Now put the value of $\dot{x}$ and v from Eqs. (2.26 & 2.24) into Eq. (2.23) it will give Lagrangian in a form

$$L = \left[A\left(x,t\right) + v_\parallel \hat{b} + v_\perp \hat{c}\right] \cdot \left[\dot{X} + \frac{d}{dt}\left(\frac{v_\perp}{B}\hat{a}\right)\right] - H\left(v,x\right) \tag{2.27}$$

Fig. 2.4 [27] demonstrates unit vectors, i.e. $\hat{a} = \cos\xi\hat{e}_1 - \sin\xi\hat{e}_2$ and $\hat{c} \times \hat{a} = \hat{b}$.

Let suppose that $v_\perp$ is very small in compression to all other space components. Hence variation occur in the field is very small and slow as compare to gyro frequency, ω_g. So vector potential $\mathbf{A}$ in term of small parameter $v_\perp$ is

$$\mathbf{A}(x,t) \cong \mathbf{A}(X,t) + \frac{v_\perp}{B}\left(\hat{a}\cdot\nabla\right)\mathbf{A}(X,t) \tag{2.28}$$

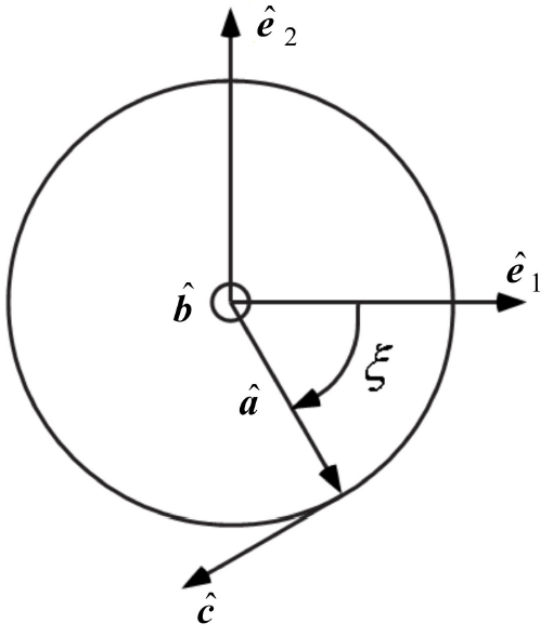

Fig. 2.8: $\hat{e}_1$,$\hat{e}_2$, $\hat{a}$,$\hat{b}$ *and* $\hat{c}$ *are unit vectors set for a charge particle circulating around* B.

Put Eq. (2.28) in Eq. (2.27), the Lagrangian become

$$\begin{aligned} L &= \left[\mathbf{A}(X,t) + \frac{v_\perp}{B}\left(\hat{a}\cdot\nabla\right)\mathbf{A}(X,t) + v_\parallel\hat{b} + v_\perp\hat{c}\right]\cdot\left[\dot{X} + \frac{d}{dt}\left(\frac{v_\perp}{B}\hat{a}\right)\right] \\ &\quad -H\left(v,x\right), \end{aligned}$$

$$\begin{aligned} L &= \left[\mathbf{A} + v_\parallel\hat{b} + v_\perp\hat{c}\right]\cdot\dot{X} + \left(\frac{v_\perp}{B}\left(\hat{a}\cdot\nabla\right)\mathbf{A}\right)\cdot\dot{X} + \mathbf{A}\cdot\frac{d}{dt}\left(\frac{v_\perp}{B}\hat{a}\right) \\ &\quad + \frac{v_\perp}{B}\left(\hat{a}\cdot\nabla\right)\mathbf{A}\cdot\frac{d}{dt}\left(\frac{v_\perp}{B}\hat{a}\right) + v_\parallel\hat{b}\cdot\frac{d}{dt}\left(\frac{v_\perp}{B}\hat{a}\right) + \\ &\quad v_\perp\hat{c}\cdot\frac{d}{dt}\left(\frac{v_\perp}{B}\hat{a}\right) - H\left(v,x\right), \end{aligned}$$

or

$$\begin{aligned} L &= \left[\mathbf{A} + v_\parallel\hat{b} + v_\perp\hat{c}\right]\cdot\dot{X} + \left(v_\parallel\hat{b} + v_\perp\hat{c}\right)\cdot\frac{d}{dt}\left(\frac{v_\perp}{B}\hat{a}\right) + \mathbf{A}\cdot\frac{d}{dt}\left(\frac{v_\perp}{B}\hat{a}\right) \\ &\quad + \left(\frac{v_\perp}{B}\hat{a}\cdot\nabla\right)\mathbf{A}\cdot\frac{d}{dt}\left(\frac{v_\perp}{B}\hat{a}\right) + \left(\left(\frac{v_\perp}{B}\hat{a}\cdot\nabla\right)\mathbf{A}\right)\cdot\dot{X} - H\left(v,x\right) \end{aligned} \tag{2.29}$$

Note that $\mathbf{A}$ used in Eq. (2.29) having coordinates of (X,t) which is related to guiding center position. Time derivative present in last equation gives

$$\frac{d}{dt}\left(v_\perp\hat{a}\right) = v_\perp\dot{\hat{a}} + \dot{v}_\perp\hat{a} = v_\perp\dot{\xi}\hat{c} + \dot{v}_\perp\hat{a} \tag{2.30}$$

From definition of unit vectors it is clear that $\dot{\hat{a}} = \dot{\xi}\hat{c}$. Therefore, second term on right hand side of Eq. (2.29) become

$$\left(v_\parallel\hat{b} + v_\perp\hat{c}\right)\cdot\frac{d}{dt}\left(\frac{v_\perp}{B}\hat{a}\right) = \frac{1}{B}\left(v_\parallel\hat{b} + v_\perp\hat{c}\right)\cdot\left(v_\perp\dot{\xi}\hat{c} + \dot{v}_\perp\hat{a}\right) = \frac{v_\perp^2\dot{\xi}}{B}\ . \tag{2.31}$$

We know that Lagrangian remain unchanged after taking its exact time derivative, the same technique can be executed to any order [24, 28]. To modify Lagrangian of Eq. (2.29), take a function S from [24] as

$$S = -\frac{v_\perp}{B}\hat{a}\cdot\mathbf{A}\ . \tag{2.32}$$

After taking its time derivative it can be written as

$$\frac{dS}{dt} = -\frac{1}{B}\frac{d}{dt}\left(v_\perp \hat{a}\cdot\mathbf{A}\right)$$

$$\frac{dS}{dt} = -\frac{1}{B}\left(\dot{v}_\perp \hat{a}\cdot\mathbf{A} + v_\perp \dot{\hat{a}}\cdot\mathbf{A} + v_\perp \hat{a}\cdot\dot{\mathbf{A}}\right) \tag{2.33}$$

Differentiate $\mathbf{A}$ with respect to time, one finds

$$\dot{\mathbf{A}} = \frac{\partial \mathbf{A}}{\partial t} + \left(\dot{X}\cdot\nabla\right)\mathbf{A} \tag{2.34}$$

Substituting Eq. (2.34) in Eq. (2.33), it yields

$$\frac{dS}{dt} = -\frac{\dot{v}_\perp}{B}\hat{a}\cdot\mathbf{A} - \frac{v_\perp}{B}\dot{\hat{a}}\cdot\mathbf{A} - \frac{v_\perp}{B}\hat{a}\cdot\left(\frac{\partial \mathbf{A}}{\partial t} + \left(\dot{X}\cdot\nabla\right)\mathbf{A}\right)$$

$$\frac{dS}{dt} = -\frac{\dot{v}_\perp}{B}\hat{a}\cdot\mathbf{A} - \frac{v_\perp}{B}\dot{\hat{a}}\cdot\mathbf{A} - \frac{v_\perp}{B}\hat{a}\cdot\frac{\partial \mathbf{A}}{\partial t} - \frac{v_\perp}{B}\hat{a}\cdot\left(\dot{X}\cdot\nabla\right)\mathbf{A}\ . \tag{2.35}$$

Adding Eq. (2.35) in Eq. (2.29) the Lagrangian become

$$\begin{aligned} L \;=\; & \left[\mathbf{A} + v_\parallel \hat{b} + v_\perp \hat{c}\right]\cdot\dot{X} + \frac{v_\perp^2 \dot{\xi}}{B} + \frac{\mathbf{A}}{B}\cdot\left(v_\perp \dot{\xi}\hat{c} + \dot{v}_\perp \hat{a}\right) \\ & + \left(\frac{v_\perp}{B^2}\left(\hat{a}\cdot\nabla\right)\mathbf{A}\right)\cdot\left(v_\perp\dot{\xi}\hat{c} + \dot{v}_\perp\hat{a}\right) + \frac{v_\perp}{B}\left(\hat{a}\cdot\nabla\right)\mathbf{A}\cdot\dot{X} - \frac{\dot{v}_\perp}{B}\hat{a}\cdot\mathbf{A} \\ & - \frac{v_\perp\dot{\xi}}{B}\hat{c}\cdot\mathbf{A} - \frac{v_\perp}{B}\hat{a}\cdot\frac{\partial\mathbf{A}}{\partial t} - \frac{v_\perp}{B}\hat{a}\cdot\left(\dot{X}\cdot\nabla\right)\mathbf{A} - H\left(v,x\right) \end{aligned}$$

or

$$\begin{aligned} L \;=\; & \left[\mathbf{A} + v_\parallel \hat{b} + v_\perp \hat{c}\right]\cdot\dot{X} + \frac{v_\perp^2\dot{\xi}}{B} + \dot{v}_\perp\frac{\mathbf{A}\cdot\hat{a}}{B} + v_\perp\dot{\xi}\frac{\mathbf{A}\cdot\hat{c}}{B} \\ & + \frac{v_\perp^2\dot{\xi}}{B^2}\left(\hat{a}\cdot\nabla\right)\mathbf{A}\cdot\hat{c} + \frac{v_\perp\dot{v}_\perp}{B^2}\left(\hat{a}\cdot\nabla\right)\mathbf{A}\cdot\hat{a} + \frac{v_\perp}{B}\left(\hat{a}\cdot\nabla\right)\mathbf{A}\cdot\dot{X} \\ & - \dot{v}_\perp\frac{\mathbf{A}\cdot\hat{a}}{B} - v_\perp\dot{\xi}\frac{\mathbf{A}\cdot\hat{c}}{B} - \frac{v_\perp}{B}\hat{a}\cdot\frac{\partial\mathbf{A}}{\partial t} - \frac{v_\perp}{B}\hat{a}\cdot\left(\dot{X}\cdot\nabla\right)\mathbf{A} \\ & - H\left(v,x\right) \end{aligned}$$

On further simplification some terms will cancel and we are left with

$$
\begin{aligned}
L &= \left[\mathbf{A} + v_{\parallel}\hat{b} + v_{\perp}\hat{c}\right]\cdot\dot{X} + \frac{v_{\perp}^{2}\dot{\xi}}{B} + \frac{v_{\perp}^{2}\dot{\xi}}{B^{2}}\left(\hat{a}\cdot\nabla\right)\mathbf{A}\cdot\hat{c} \\
&\quad + \frac{v_{\perp}\dot{v}_{\perp}}{B^{2}}\left(\hat{a}\cdot\nabla\right)\mathbf{A}\cdot\hat{a} - \frac{v_{\perp}}{B}\hat{a}\cdot\frac{\partial\mathbf{A}}{\partial t} - H\left(v,x\right)\ .
\end{aligned}
\tag{2.36}
$$

Now again add an exact derivative of a function S_1 to Eq. (2.36), in this case S_1 is the form [24, 26]

$$
S_1 = -\frac{v_{\perp}^{2}}{2B^{2}}\left(\hat{a}\cdot\nabla\right)\mathbf{A}\cdot\hat{a} \tag{2.37}
$$

Differentiate it with respect to time.

$$
\frac{dS_1}{dt} = -\frac{1}{2B^{2}}\left[2v_{\perp}\dot{v}_{\perp}\left(\hat{a}\cdot\nabla\right)\mathbf{A}\cdot\hat{a} + v_{\perp}^{2}\frac{dI_1}{dt}\right], \tag{2.38}
$$

where I_1 is

$$
I_1 = \left(\hat{a}\cdot\nabla\right)\mathbf{A}\cdot\hat{a}\ .
$$

Take time derivative of I_1.

$$
\frac{dI_1}{dt} = \left[\frac{d}{dt}\left(\hat{a}\cdot\nabla\right)\right]\mathbf{A}\cdot\hat{a} + \hat{a}\cdot\nabla\left[\dot{\mathbf{A}}\cdot\hat{a} + \mathbf{A}\cdot\dot{\hat{a}}\right]
$$

Introduce value of $\dot{\hat{a}}$ and rearrange to find

$$
\frac{dI_1}{dt} = \dot{\xi}\left(\hat{c}\cdot\nabla\right)\mathbf{A}\cdot\hat{a} + \left(\hat{a}\cdot\nabla\right)\dot{\mathbf{A}}\cdot\hat{a} + \dot{\xi}\left(\hat{a}\cdot\nabla\right)\mathbf{A}\cdot\hat{c} \tag{2.39}
$$

using Eq. (2.39) in Eq. (2.38), the expression takes the form

$$
\begin{aligned}
\frac{dS_1}{dt} &= -\frac{v_{\perp}\dot{v}_{\perp}}{B^{2}}\left(\hat{a}\cdot\nabla\right)\mathbf{A}\cdot\hat{a} - \frac{v_{\perp}^{2}\dot{\xi}}{2B^{2}}\left(\hat{c}\cdot\nabla\right)\mathbf{A}\cdot\hat{a} - \frac{v_{\perp}^{2}}{2B^{2}}\left(\hat{a}\cdot\nabla\right)\dot{\mathbf{A}}\cdot\hat{a} \\
&\quad - \frac{v_{\perp}^{2}\dot{\xi}}{2B^{2}}\left(\hat{a}\cdot\nabla\right)\mathbf{A}\cdot\hat{c}
\end{aligned}
\tag{2.40}
$$

Add Eq. (2.40) in Eq. (2.36), to get

$$
\begin{aligned}
L &= \left[\mathbf{A} + v_{\parallel}\hat{b} + v_{\perp}\hat{c}\right]\cdot\dot{X} + \frac{v_{\perp}^2\dot{\xi}}{B} + \frac{v_{\perp}^2\dot{\xi}}{B^2}\left(\hat{a}\cdot\nabla\right)\mathbf{A}\cdot\hat{c} \\
&\quad + \frac{v_{\perp}\dot{v}_{\perp}}{B^2}\left(\hat{a}\cdot\nabla\right)\mathbf{A}\cdot\hat{a} - \frac{v_{\perp}}{B}\hat{a}\cdot\frac{\partial\mathbf{A}}{\partial t} - H\left(v,x\right) - \frac{v_{\perp}\dot{v}_{\perp}}{B^2}\left(\hat{a}\cdot\nabla\right)\mathbf{A}\cdot\hat{a} \\
&\quad - \frac{v_{\perp}^2\dot{\xi}}{2B^2}\left(\hat{c}\cdot\nabla\right)\mathbf{A}\cdot\hat{a} - \frac{v_{\perp}^2}{2B^2}\left(\hat{a}\cdot\nabla\right)\dot{\mathbf{A}}\cdot\hat{a} - \frac{v_{\perp}^2\dot{\xi}}{2B^2}\left(\hat{a}\cdot\nabla\right)\mathbf{A}\cdot\hat{c}
\end{aligned}
$$

some terms will cancel out

$$
\begin{aligned}
L &= \left[\mathbf{A} + v_{\parallel}\hat{b} + v_{\perp}\hat{c}\right]\cdot\dot{X} + \frac{v_{\perp}^2\dot{\xi}}{B} + \frac{v_{\perp}^2\dot{\xi}}{B^2}\left(\hat{a}\cdot\nabla\right)\mathbf{A}\cdot\hat{c} - \frac{v_{\perp}}{B}\hat{a}\cdot\frac{\partial\mathbf{A}}{\partial t} \\
&\quad - \frac{v_{\perp}^2\dot{\xi}}{2B^2}\left(\hat{c}\cdot\nabla\right)\mathbf{A}\cdot\hat{a} - \frac{v_{\perp}^2}{2B^2}\left(\hat{a}\cdot\nabla\right)\dot{\mathbf{A}}\cdot\hat{a} - \frac{v_{\perp}^2\dot{\xi}}{2B^2}\left(\hat{a}\cdot\nabla\right)\mathbf{A}\cdot\hat{c} \\
&\quad - H\left(v,x\right)
\end{aligned}
$$

or

$$
\begin{aligned}
L &= \left[\mathbf{A} + v_{\parallel}\hat{b} + v_{\perp}\hat{c}\right]\cdot\dot{X} + \frac{v_{\perp}^2\dot{\xi}}{B} - \frac{v_{\perp}}{B}\hat{a}\cdot\frac{\partial\mathbf{A}}{\partial t} - \frac{v_{\perp}^2}{2B^2}\left(\hat{a}\cdot\nabla\right)\dot{\mathbf{A}}\cdot\hat{a} \\
&\quad + \frac{v_{\perp}^2\dot{\xi}}{2B^2}\left[\left(\hat{a}\cdot\nabla\right)\mathbf{A}\cdot\hat{c} - \left(\hat{c}\cdot\nabla\right)\mathbf{A}\cdot\hat{a}\right] - H\left(v,x\right)
\end{aligned}
\tag{2.41}
$$

With reference to Eq. (2.28) we drop all second order and higher order terms of $v_{\perp}$ except having product with faster term $\dot{\xi}$, due to this reason we are going to drop the fourth term of last equation. Further using the identity [24]

$$
\left(\hat{a}\cdot\nabla\right)\mathbf{A}\cdot\hat{c} - \left(\hat{c}\cdot\nabla\right)\mathbf{A}\cdot\hat{a} = -B \tag{2.42}
$$

Simplifies Eq. (2.41) to form

$$
L = \left[\mathbf{A} + v_{\parallel}\hat{b} + v_{\perp}\hat{c}\right]\cdot\dot{X} + \frac{v_{\perp}^2\dot{\xi}}{2B} - \frac{v_{\perp}}{B}\hat{a}\cdot\frac{\partial\mathbf{A}}{\partial t} - H\left(v,x\right) \tag{2.43}
$$

Take average of last equation over time period of full gyration. In the result the term including $v_{\perp}\hat{c}$ and $\hat{a}\cdot\frac{\partial\mathbf{A}}{\partial t}$ diminish, and the Lagrangian reduced to the form

$$L = \left[\mathbf{A} + v_{\parallel}\hat{b}\right] \cdot \dot{X} + \frac{v_{\perp}^2 \dot{\xi}}{2B} - H\left(v, x\right) \ . \tag{2.44}$$

Inserting values for parallel gyro radius which is by definition $\rho_{\parallel} = v_{\parallel}/\mathbf{B}$, magnetic momentum i.e. $\mu = v_{\perp}^2/2\mathbf{B}$ (assuming $m = 1$) and rewrite the Lagrangian

$$L = \left[\mathbf{A} + \rho_{\parallel}\mathbf{B}\right] \cdot \mathbf{v} + \mu\dot{\xi} - H\left(v, x\right) \tag{2.45}$$

Inserting expression for vector potential $\mathbf{A}$ as define in Eq. (2.21) i.e. $A{=}\Phi\nabla\theta - \psi\nabla\zeta$ and expression for magnetic field $\mathbf{B}$ as define in Eq. (2.18), i.e. $\mathbf{B} {=} g\nabla\zeta + I\nabla\theta + k\nabla\text{Ŧ}$ the Lagrangian in flux coordinates is

$$L = \left[\Phi\nabla\theta - \psi\nabla\zeta + \rho_{\parallel}\left(g\nabla\zeta + I\nabla\theta + k\nabla\text{Ŧ}\right)\right] \cdot \mathbf{v} + \mu\dot{\xi} - H\left(v, x\right)$$

$$\begin{aligned} L \ &= \ \left(\Phi + \rho_{\parallel}I\right)\nabla\theta \cdot \mathbf{v} + \left(-\psi + \rho_{\parallel}g\right)\nabla\zeta \cdot \mathbf{v} + \rho_{\parallel}k\nabla\text{Ŧ} \\ &\quad + \mu\dot{\xi} - H\left(v, x\right) \end{aligned}$$

$$L = \left(\Phi + \rho_{\parallel}I\right)\dot{\theta} + \left(-\psi + \rho_{\parallel}g\right)\dot{\zeta} - H\left(v, x\right) + \mu\dot{\xi} + \rho_{\parallel}k\dot{\text{Ŧ}} \ . \tag{2.46}$$

First four terms of last equation clearly indicate that it is of canonical form $p_i\dot{q}_i$. ψ present in the 2nd term of last equation describes as canonical momentum. Some sort of adjustment is required if want to obtain Lagrangian in a standard canonical form, such a adjustment is carried out by 2nd order modification of guiding center position along magnetic field. In the result of this adjustment an extra term $\left[\mathbf{A}{+}\rho_{\parallel}\mathbf{B}\right] \cdot \mathbf{v}^*$ is produced in Eq. (2.45), which corresponds to a condition

$$\mathbf{A} \cdot \mathbf{v}^* {+} \rho_{\parallel}\mathbf{B} \cdot \mathbf{v}_{\perp} + \rho_{\parallel}k\dot{\text{Ŧ}} = 0 \tag{2.47}$$

with upon using the relation $\mathbf{B} \cdot \mathbf{A} = 0$, gives

$$\mathbf{v}^* = -k\dot{\text{Ŧ}}\frac{\mathbf{B}}{B^2} \tag{2.48}$$

Lagrangian in their standard canonical form become

$$L = \left(\Phi + \rho_{\|} I\right) \dot{\theta} + \left(-\psi + \rho_{\|} g\right) \dot{\zeta} + \mu \dot{\xi} - H\left(v, x\right) \tag{2.49}$$

2.2.3 Canonical coordinates

Lagrangian in their standard form has the representation

$$L = \sum_i p_i \dot{q}_i - H \ . \tag{2.50}$$

By comparing Eq. (2.49) and Eq. (2.50) it clearly indicate the canonical coordinates θ,ζ and ξ along with there canonical momenta as

$$p_\theta = \Phi + \rho_{\|} I \ , \tag{2.51}$$

$$p_\zeta = -\psi + \rho_{\|} g \tag{2.52}$$

and

$$p_\xi = \mu \ . \tag{2.53}$$

So equations of motion are

$$\dot{p}_\theta = -\frac{\partial H}{\partial \theta}, \qquad \dot{\theta} = \frac{\partial H}{\partial p_\theta} \tag{2.54}$$

$$\dot{p}_\zeta = -\frac{\partial H}{\partial \zeta}, \qquad \dot{\zeta} = \frac{\partial H}{\partial p_\zeta} \tag{2.55}$$

$$\dot{p}_\xi = -\frac{\partial H}{\partial \xi}, \qquad \dot{\xi} = \frac{\partial H}{\partial p_\xi} \tag{2.56}$$

With the Hamiltonian of the system is

$$H = \frac{1}{2}\left(\rho_{\parallel}B\right)^2 + \mu B \tag{2.57}$$

using Eq. (2.57) in Eq. (2.54) result in

$$\dot{\theta} = \frac{\partial}{\partial p_\theta}\left[\frac{1}{2}\left(\rho_{\parallel}B\right)^2 + \mu B\right]$$

$$\dot{\theta} = \rho_{\parallel}B\left[B\frac{\partial \rho_{\parallel}}{\partial p_\theta} + \rho_{\parallel}\frac{\partial B}{\partial p_\theta}\right] + \mu\frac{\partial B}{\partial p_\theta}$$

$$\dot{\theta} = \rho_{\parallel}B^2\frac{\partial \rho_{\parallel}}{\partial p_\theta} + \frac{\partial B}{\partial p_\theta}\left(\rho_{\parallel}^2 B + \mu\right)$$

$$\dot{\theta} = \rho_{\parallel}B^2\frac{\partial \rho_{\parallel}}{\partial p_\theta} + \frac{\partial B}{\partial \psi}\frac{\partial \psi}{\partial p_\theta}\left(\rho_{\parallel}^2 B + \mu\right) \tag{2.58}$$

Expression for $\frac{\partial \rho_{\parallel}}{\partial p_\theta}$ can be calculated from Eq. (2.52) as

$$\frac{\partial \rho_{\parallel}}{\partial p_\theta} = \frac{\partial}{\partial p_\theta}\left[\frac{p_\zeta + \psi}{g}\right]$$

$$\frac{\partial \rho_{\parallel}}{\partial p_\theta} = \frac{g\frac{\partial}{\partial p_\theta}\left[p_\zeta + \psi\right] - \frac{\partial g}{\partial p_\theta}\left[p_\zeta + \psi\right]}{g^2}$$

$$\frac{\partial \rho_{\parallel}}{\partial p_\theta} = \frac{g\frac{\partial \psi}{\partial p_\theta} - \frac{\partial g}{\partial \psi}\frac{\partial \psi}{\partial p_\theta}\rho_{\parallel}g}{g^2} \tag{2.59}$$

Using expression for $\frac{\partial \rho_{\parallel}}{\partial p_\theta}$ from last equation in Eq. (2.58) we find

$$\dot{\theta} = \rho_{\parallel}B^2\left[\frac{g\frac{\partial \psi}{\partial p_\theta} - \frac{\partial g}{\partial \psi}\frac{\partial \psi}{\partial p_\theta}\rho_{\parallel}g}{g^2}\right] + \frac{\partial B}{\partial \psi}\frac{\partial \psi}{\partial p_\theta}\left(\rho_{\parallel}^2 B + \mu\right) \tag{2.60}$$

Using Eq. (2.51) and Eq. (2.52), one finds expression for $\frac{\partial \psi}{\partial p_\theta}$, i.e.

$$\frac{p_\theta - \Phi}{I} = \rho_{\parallel}$$

$$\frac{p_\zeta + \psi}{g} = \rho_{\parallel}$$

compare the above equations

$$g\left(p_\theta - \Phi\right) = I\left(p_\zeta + \psi\right) \tag{2.61}$$

Differentiate Eq. (2.61) partially with respect to p_θ and then again using Eq. (2.51) and Eq. (2.52) we obtain

$$g - g\frac{\partial \Phi}{\partial p_\theta} + \rho_\parallel I \frac{\partial g}{\partial p_\theta} = I\frac{\partial \psi}{\partial p_\theta} + \rho_\parallel g \frac{\partial I}{\partial p_\theta} \tag{2.62}$$

Interpreting $\frac{\partial}{\partial p_\theta} = \frac{\partial \psi}{\partial p_\theta}\frac{\partial}{\partial \psi}$ we get

$$g - g\frac{\partial \Phi}{\partial \psi}\frac{\partial \psi}{\partial p_\theta} + \rho_\parallel \left(\frac{\partial I}{\partial \psi} g - I\frac{\partial g}{\partial \psi}\right)\frac{\partial \psi}{\partial p_\theta} = I\frac{\partial \psi}{\partial p_\theta} \tag{2.63}$$

$$g = \frac{\partial \psi}{\partial p_\theta}\left[-\rho_\parallel \left(\frac{\partial I}{\partial \psi} g - I\frac{\partial g}{\partial \psi}\right) + q_s g + I\right] \tag{2.64}$$

and finally

$$\frac{\partial \psi}{\partial p_\theta} = \frac{g}{\mathcal{G}} \,, \tag{2.65}$$

where $\mathcal{G}$ is

$$\mathcal{G} = -\rho_\parallel \left(\frac{\partial I}{\partial \psi} g - I\frac{\partial g}{\partial \psi}\right) + q_s g + I \tag{2.66}$$

Putting Eq. (2.65) in Eq. (2.60) final equation for $\dot{\theta}$ is

$$\dot{\theta} = \rho_\parallel B^2 \left(\frac{I - \rho_\parallel \acute{g}}{\mathcal{G}}\right) + \frac{\partial B}{\partial \psi}\frac{\partial \psi}{\partial p_\theta}\left(\mu + \rho_\parallel^2 B\right)$$

$$\dot{\theta} = \rho_\parallel B^2 \left(\frac{I - \rho_\parallel \acute{g}}{\mathcal{G}}\right) + \frac{g}{\mathcal{G}}\frac{\partial B}{\partial \psi}\left(\mu + \rho_\parallel^2 B\right)$$

$$\dot{\theta} = \rho_\parallel B^2 \left(\frac{I - \rho_\parallel \acute{g}}{\mathcal{G}}\right) + \left(\mu + \rho_\parallel^2 B\right)\frac{g}{\mathcal{G}}\frac{\partial B}{\partial \psi} \tag{2.67}$$

The above method is also use to derive equation for $\dot{\zeta}$ which is as follow

$$\dot{\zeta} = \rho_\parallel B^2 \left(\frac{q_s + \rho_\parallel I^{'}}{\mathcal{G}}\right) - \left(\mu + \rho_\parallel^2 B\right)\frac{1}{\mathcal{G}}\frac{\partial B}{\partial \psi} \tag{2.68}$$

It is clear that $\rho_{\|}$ is p_θ and p_ζ dependant only, so to find expression for $\dot{p}_\theta$ introduce Hamiltonian of Eq. (2.57) in Eq. (2.54) it will

$$\dot{p}_\theta = -\frac{\partial}{\partial\theta}\left[\frac{1}{2}\left(\rho_{\|}B\right)^2 + \mu B\right]$$

$$\dot{p}_\theta = -\rho_{\|}B\left(B\frac{\partial\rho_{\|}}{\partial\theta} + \rho_{\|}\frac{\partial B}{\partial\theta}\right) - \mu\frac{\partial B}{\partial\theta}$$

$$\dot{p}_\theta = -\rho_{\|}B^2\frac{\partial\rho_{\|}}{\partial\theta} - \rho_{\|}^2 B\frac{\partial B}{\partial\theta} - \mu\frac{\partial B}{\partial\theta}$$

As $\rho_{\|}$ is independent of θ, so first term in the last equation will be vanish and the last equation can be rewrite as

$$\dot{p}_\theta = -\left(\mu + \rho_{\|}^2 B\right)\frac{\partial B}{\partial\theta} \tag{2.69}$$

and similarly

$$\dot{p}_\zeta = -\left(\mu + \rho_{\|}^2 B\right)\frac{\partial B}{\partial\zeta} \tag{2.70}$$

Hamiltonian equations of motion can be worked out by using our code based on SIA. To study magnetic field and its perturbations analytically it is far better to suppose low-β plasma and the fusion reactor having large aspect ratio having circular magnetic flux surfaces.

Chapter 3

Method of Symplectic integration

In this chapter we discuss the numerical integration of Hamiltonian dynamical system by using numerical integration technique like symplectic integration algorithm and Range-Kutta algorithm (RKA), a non-symplectic integration technique [8], and to check their behaviors, i.e. its stability with long time period and energy preservations [28, 29]. For all these illustrations Henon-Heiles Hamiltonian have been used [30].

3.1 Integration of Hamiltonian System

The system which is completly describe by Hamilton equations are called Hamiltanion system. Hamiltonian is the sum of the kinetic and potential energies expressed as a function of positions and their conjugate momenta.

By using different numerical techniques it's easy to exactly integrate canonical equations of motion (first order partial differential equations) for a dynamical Hamiltonian system. Checking the conservations of Poincaré characteristics is very important for the judgment of these numerical simulation techniques that how much these techniques show stability toward long time simulations.

For Hamiltonian system if the integration were performed for long period of time through Rangue-Kutta integration technique, error in energy increases step by step, i.e. energy is not conserved here and this reason make it structurally unstable against the numerical perturbation. This drawback of Rangue-Kutta integration technique converges our attentions to an unusual

property, i.e. when Hamiltonian system is integrated for huge number of step with Rangue-Kutta integration technique it may become like non-Hamiltonian system.

The problems with the non-symplectic RK integration provide a gateway to the introduction new numerical integration technique, the symplectic integration algorithm for Hamiltonian systems. Where no change occur in energy after each integration step, i.e. that energy is conserved. By arranging each step of integration by symplectic transformation the characteristics of the Hamiltonian system is conserve. A Symplectic transformation satisfies the condition

$$M^T(q,p)JM(q,p) = J, \tag{3.1}$$

where M is the Jacobian of transformation , q and p are vectors of canonical conjugate coordinates and J is the standard Symplectic matrix given by

$$\begin{bmatrix} 0 & I \\ -I & 0 \end{bmatrix} . \tag{3.2}$$

Here I is the identity matrix. Eq. (3.1) is the *symplectic condition.*

Sympletic condition for canonical transformation is an important tool to check that the given transformation is canonical or not. Canonical transformations play an important role in Hamiltonian dynamics. In non-sympletic numerical integration algorithm (NSIA) process there is no such limitation even if the energy conservation is built into the algorithm. The only limitation on the NSIAs is to investigate for short interval of time and that's why due to the Hamiltonian nature of the dynamics we miss global structure. In short all problems in NSIAs arises when integration is carried out for large period of time, NSIAs are effective in short time examination. In SIA, from one time step to the next we go by canonical transformation like

$$\underbrace{p(t_i), q(t_i)}_{old\ coordinates} \xrightarrow{canonical} \underbrace{p(t_i+\delta t), q(t_i+\delta t)}_{new\ coordinates}$$

Different SIAs can be formulated depending on how the time map of Hamiltonian system is approximated and matched with the generating function map. In long time simulation of the dynamics system symplectic integration method are favorable.

3.2 Symplectic integration of a general Hamiltonian system

Hamilton-Jacobi equations give an idea for the solution of a general Hamiltonian, the NSIA in this case is very complex and can not handle easily [8]. Such problems motivate us toward the development and implementation of such new computational technique which have the quality to handle general Hamiltonian easily, i.e. to describe equation of motions of n-dimensional system for general Hamiltonian funcation $H(P,Q)$. Transformation equations can be carried out by using generating function of 3rd kind [28], $G(p,Q) = G(p_1,...,p_i;Q_1,...,Q_i)$,

$$P_i = -\frac{\partial G}{\partial Q_i} \tag{3.3}$$

and

$$q_i = -\frac{\partial G}{\partial p_i} \tag{3.4}$$

The generating function can be expand as

$$G(p,Q) = \sum_{m=0}^{\infty} \frac{\delta t^m}{m!} G_m(p,Q), \tag{3.5}$$

where $G_0 = -\mathbf{p}.\mathbf{Q}$ gives the identity transformation and δt is the time step. Using Eq. (3.5) in Eq. (3.3) it follows

$$P_i = p_i + \sum_{m=1}^{\infty} \frac{\delta t^m}{m!} P_m(p,Q) \tag{3.6}$$

with

$$P_m = -\frac{\partial G_m(p,Q)}{\partial Q_m} \tag{3.7}$$

For Hamiltonian function the canonical equation of motion are

$$\dot{P}_i = -\frac{\partial H}{\partial Q_i} \tag{3.8}$$

and

$$\dot{Q}_i = \frac{\partial H}{\partial P_i} \tag{3.9}$$

The time derivative of P is given by

$$P_i = \frac{\partial P_i}{\partial t} + \frac{\partial P_i}{\partial Q_i} \cdot \dot{Q}_i \tag{3.10}$$

Putting the expression for P from Eq. (3.10) in Eqs. (3.8) and Eq. (3.9) yields the expression [9]

$$\sum_{m=1}^{\infty} \frac{P_m \delta t^{m-1}}{(m-1)!} + \sum_{m=1}^{\infty} \frac{\partial t^m}{m!} \frac{\partial P_m}{\partial Q_m} \cdot \dot{Q}_m = -\frac{\partial H}{\partial Q_i}(p + \sum_{m=1}^{\infty} \frac{P_m \delta t^m}{m!}, Q) \tag{3.11}$$

Defining

$$\Delta P = \sum_{m=1}^{\infty} \frac{\delta t^m}{m!} P_m(p, Q) \tag{3.12}$$

The argument $P_i = p_i + ... = p_i + \Delta P$ in the Hamiltonian can be expend using Taylor series, it takes the form

$$\begin{aligned} \sum_{m=0}^{\infty} \frac{P_{m+1} \delta t^m}{m!} &= \sum_{m=1}^{\infty} \frac{\delta t^m}{m!} \frac{\partial^2 G_m}{\partial Q_m \partial Q_m} \cdot \left[\sum_{l=0}^{\infty} \frac{(\Delta P \cdot \frac{\partial}{\partial P})^l}{l!} \right] \frac{\partial H}{\partial P} \\ &\quad - \sum_{t=0}^{\infty} \frac{(\Delta P \cdot \frac{\partial}{\partial p})^1}{l!} \frac{\partial H}{\partial Q_i} \end{aligned} \tag{3.13}$$

For expanding several power of P we have to use binomial theorem and then equating the coefficients of same powers ∂t in Eq. (3.13). Depending on the power m considered, this comparison yields [9],

$$\begin{aligned} \frac{\partial G_{m+1}}{\partial Q} &= -m! \sum_{s=1}^{s} \frac{1}{s!} \frac{\partial^2 G}{\partial Q_s \partial Q_s} \cdot \sum_{l=0}^{m-s} \sum_{\substack{r_1,...,r_m=0 \\ \sum r_i = l \\ \sum i r_i = m-s}} \frac{1}{r_1!...r_m} \\ &\quad \times \left(\frac{P_1}{1!} \cdot \frac{\partial}{\partial p} \right)^{r_1} ... \left(\frac{P_m}{m!} \cdot \frac{\partial}{\partial p} \right)^{r_m} \frac{\partial H}{\partial p} \\ &\quad + m! \sum_{s=0}^{m} \sum_{\substack{r_1,...,r_m=0 \\ \sum r_i = s \\ \sum i r_i = m}} \frac{1}{r_1!...r_m!} \left(\frac{P_1}{1!} \cdot \frac{\partial}{\partial p} \right)^{r_1} ... \left(\frac{P_m}{m!} \cdot \frac{\partial}{\partial p} \right)^{r_m} \frac{\partial H}{\partial q} \end{aligned} \tag{3.14}$$

For $m = 0, 1, 2, ...$ the right hand side of Eq. (3.14) will be partial derivatives with respect

to q and is used to calculate G to any desired order, e.g.

$$G_1 = H \tag{3.15}$$

$$G_2 = -\sum_i^n \frac{\partial H}{\partial p_i} \cdot \frac{\partial G_1}{\partial Q_i} \tag{3.16}$$

$$G_3 = -\sum_i^n \left[\frac{\partial H}{\partial p_i} \cdot \frac{\partial G_2}{\partial Q_i} - \frac{\partial G_1}{\partial Q_i} \cdot \sum_{j=1}^n \frac{\partial G_1}{\partial Q_j} \frac{\partial^2 H}{\partial p_i \partial p_j} \right] \tag{3.17}$$

$$G_4 = -\sum \left[\begin{array}{c} -\frac{\partial G_3}{\partial Q_i} \cdot \frac{\partial H}{\partial p_i} + 3 \sum_{i,j=1}^n \frac{\partial G_1}{\partial Q_i} \frac{\partial G_1}{\partial Q_j} \frac{\partial^2 H}{\partial p_i \partial p_j} \\ -\sum_{i,j,k=1}^n \frac{\partial G_1}{\partial Q_i} \frac{\partial G_1}{\partial Q_j} \frac{\partial G_1}{\partial Q_k} \frac{\partial^3 H}{\partial p_i \partial p_j \partial p_k} \end{array} \right] \tag{3.18}$$

Now if we want to calculate Q_i as a sum over time step expressions we have to use G_m. Using Eq. (3.5) in Eq. (3.4) to write

$$Q_i = q_i + \sum_{m=1}^{\infty} \frac{\delta t^m}{m!} \frac{\partial G_m(p, Q)}{\partial p_i} \tag{3.19}$$

Iteration method is used to solve Eq. (3.19) . During each iteration step the precedent Q is introduce again on the right hand side of the equation. The iteration terminates when Q changes by less than some specific tolerance. The value of P can easily be found by evaluating Eq. (3.6). Flow chart of SIA algorithm is shown in the Fig. 3.1

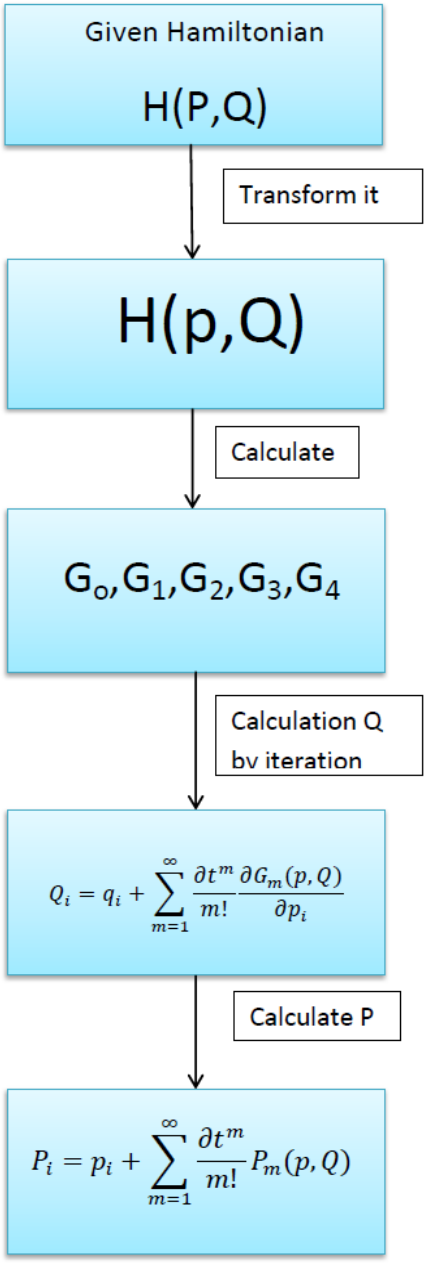

Figure 3.1: *Flow chart of SIA algorithm*

3.3 Application of SIA to Henon-Heiles Hamiltonian : *Motion of stars about a galactic center*

In order to check the behaviors of the SIA discuss in the last portion we try out the analytically simple Hamiltonian function that describes the motion of star about it's galactic center, presented by the Henon and Heiles [30]. First of all this problem was solved through non-symplectic integration technique for small time period. Later on Poincaré map of this motion of stars was presented by Channel and Scovel [8] showing long-term stability of phase space structure. Now the main aim of this portion is to find the trajectories of stars by using SIA and RKA techniques for some specific initial conditions and then compare these trajectories to check the efficiency of these techniques. As in [8, 30] from our analysis use the Hamiltonian

$$H(p,Q) = \frac{1}{2}\left(Q_1^2 + Q_2^2 + p_1^2 + p_2^2\right) + Q_1^2 Q_2 - \frac{1}{3}Q_2^3 \tag{3.20}$$

Taking Eq. (3.5) up to fourth order and introducing Eq. (3.20) in Eqs. (3.15-3.18), one finds the generation functions

$$G = \sum_{m=0}^{4} \frac{\delta t^m}{m!} G_m\left(p_o, q\right) \tag{3.21}$$

with

$$G_0 = p_1 Q_1 - p_2 Q_2, \tag{3.22}$$

$$G_1 = \frac{1}{2}\left(Q_1^2 + Q_2^2 + p_1^2 + p_2^2\right) + Q_1^1 Q_2 - \frac{1}{3}Q_2^3, \tag{3.23}$$

$$G_2 = p_1\left(Q_1 - 2Q_1 Q_2\right) + p_2(-Q_1^2 + Q_2^2 - Q_2), \tag{3.24}$$

$$\begin{aligned} G_3 \;=\; & p_1\left(2p_2 Q_1 - p_1\left(-1 - 2Q_2\right)\right) + \left(1 - 2Q_2\right) + \left(1 + 2Q_2\right) \\ & + p_2\left(2p_1 Q_1 - p_2\left(-1 + 2Q_2\right)\right), \end{aligned} \tag{3.25}$$

$$\begin{aligned} G_4 \;=\; & -4p_1 p_2 + p_2\left(-2p_1 + 2p_2\right) + 3\left(-2p_2 Q_1 + p_1\left(-1 - 2Q_2\right)\right)\left(Q_1 + 2Q_1 Q_2\right) \\ & + \left(Q_1^2 + Q_2 - Q_2^2\right)\left(-2p_1 Q_1 + p_2\left(-1 + 2Q_2\right)\right) \end{aligned} \tag{3.26}$$

Upon that Eq. (3.19) and Eq. (3.6) can be evaluated to determine the trajectory in the phase space append by the canonical variables P and Q.

The surface-of-section technique (SST) also named as Poincaré mapping is used for the graphical description of trajectories. In this technique n-dimensional trajectory is represented in $(n-1)$ dimensional space. Here the normalize space coordinate q_2 and normalize momentum p_2 are plotted under a specific condition, i.e. when the trajectory intersects the hyperplane $q_1 = 0$. It should be kept in mind that remaining momentum coordinate p_1 is a dependent coordinate, and its value can be calculated using Eq. (3.20).

3.3.1 Comparison of SIA and RKA

It is better to use surface-of-section technique to study the manner of stars trajectories around their galactic center. Poincaré maps are shown in the Figs. 3.2a and 3.2b, results in using 4th order SIA and 4th order Runge-Kutta simulations techniques. In both cases simulations results were taken for the total time period of 2.0×10^4(a.u) with time steps of 0.017.

Both graphs of Fig. 3.2 are obtain by using same initial condition as well as for same total energy H, i.e. $(q_1, q_2, p_1, p_2)_{initial} = (0.12, 0.12, 0.12, 0.12)$ and $H = 0.029952$ (a.u). It is clear from Fig. 3.1a, that for a very large number of time steps SIA gives a very fine trajectory of star motion having well defined knife edges. While on the other hand for same number of time steps star trajectory obtain by using RKA is fuzzy and having not well defined edges.

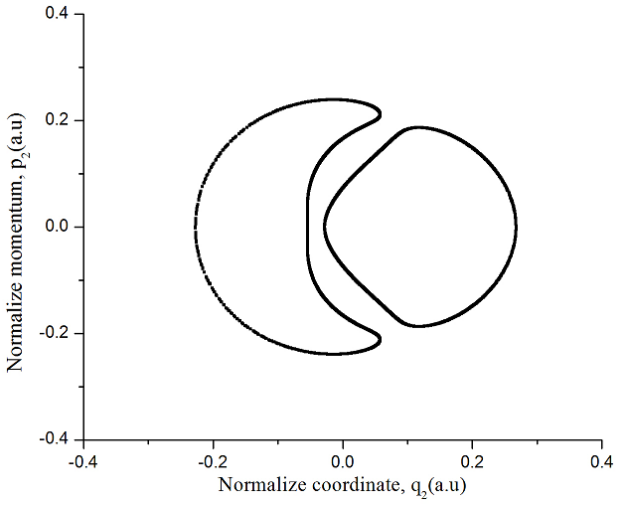

(a)

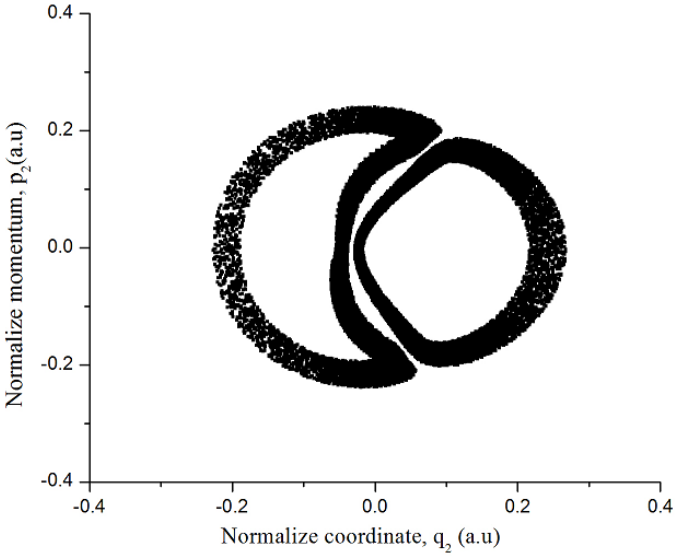

(b)

Figure 3.2: *Comparison of Poincaré maps for Henon-Heiles system with initial conditions* $(q_1, q_2, p_1, p_2)_{initial} = (0.12, 0.12, 0.12, 0.12)$ *and total energy* 0.029952 *by using (a) 4th order SIA and (b) 4th order RKA.*

Figure. 3.3 also demonstrate that Poincaré map of star motion trajectory get through SAI simulation is quite well defined and accurate while after using RKA simulations the trajectory is not much clear and foggy this is due to the fact that phase space points disperse widely around the exact trajectory. Both the Poincaré maps of Fig. 3.3 results by using same initial conditions $(q_1, q_2, p_2)_{initial} = (0, 0, 0)$ and value of p_1 can be calculated by using Eq. (3.20), in this case $(p_1)_{initial} = \sqrt{2H}$. Preferred total energy is 0.150 (a.u) and total period of time is 1.0×10^5 (a.u) with time steps $\delta t = 0.03$.

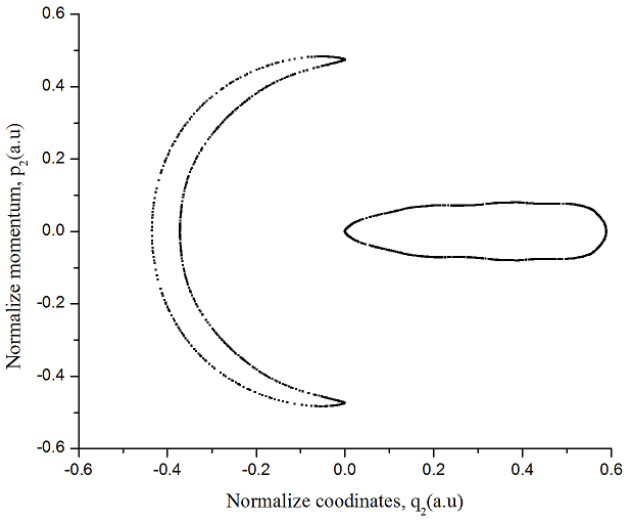

(a)

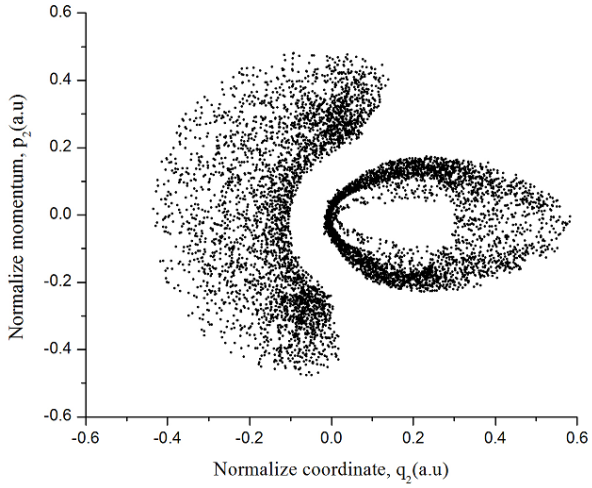

(b)

Figure 3.3: *Phase space contours comparison for Henon-Heiles system using (a) 4th order SIA and (b) 4th order RKA for initial conditions* $(q_1, q_2, p_2)_{initial} = (0, 0, 0)$ *and* $H = 0.150$.

After studying the above Figures it is concluded that for long period of time, energy is conserved in case of SIA, means that no such change occur after each step or for long time integrations errors do not increases. Due to this fact SIA got much importance for long time simulations and that why we get a well defined Poincaré maps in the result of SIA. While in case of RKA a non-symplectic integration scheme the energy is not conserved, energy error increases after each step which is the basic disadvantage of this scheme and due to this fact Poincaré maps results from RKA is not well defined.

3.3.2 Sensitivity of SIA and RKA

In this section we highlight the sensitivity of SIA and RKA. To study the behaviors of SIA and RKA after bringing a slight change in initial conditions, total energy and how trajectories changes with it.

Poincaré map shown in Fig. 3.4(a) obtain through SAI simulation technique and phase space contour displayed in Fig. 3.3(b) results from RKA, both for initial conditions of $(q_1, q_2, p_2)_{initial} = (0, 0, 0)$ and total energy 0.12000 (a.u). But if a slight change occur in total energy, i.e. 0.1592, then by using SIA we get Fig. 3.4(c), where the trajectory is ergodic over huge area and ignore some embedded regions, while for the same energy RKA shows no effect and the Poincaré map will remains same as that of Fig 3.3(b).

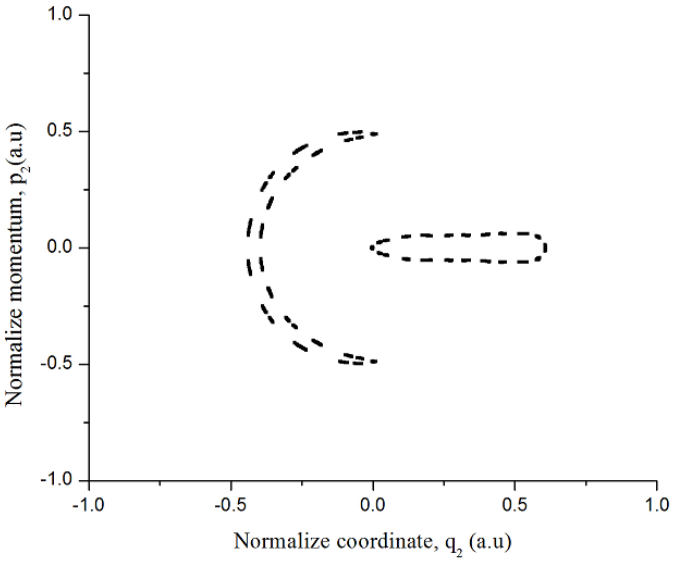
1.0
0.5
0.0
-0.5
-1.0
-1.0
-0.5
0.0
0.5
1.0
Normalize momentum, p2(a.u)
Normalize coordinate, q2 (a.u)

(a)

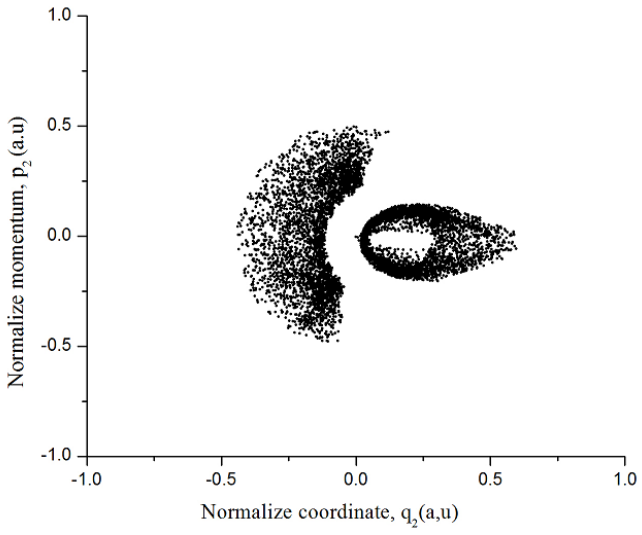
1.0
0.5
0.0
-0.5
-1.0
-1.0
-0.5
0.0
0.5
1.0
Normalize momentum, p2 (a.u)
Normalize coordinate, q2(a,u)

(b)

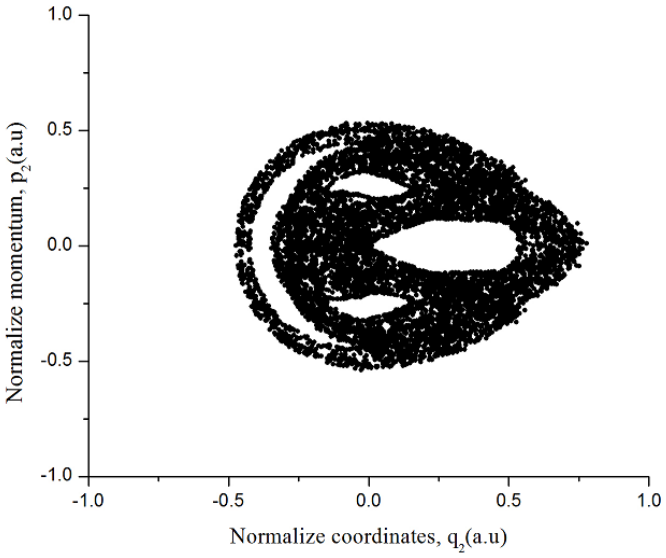

(c)

Figure 3.4: *Pioncare maps of Henon-Helies system for initial conditions of* $(q_1, q_2, p_2)_{initial} = (0, 0, 0)$ *and* p_1 *is calculated from total energy. (a) and (b) total energy is 0.12000; for (c) total energy is 0.1592.*

Poincaré maps shown in Fig. 3.5 again clearly indicates how SIA can sence change in energy in contrast to RKA. Here we used $(q_1, q_2, p_2)_{initial} = (0, 0, 0)$ and total energies of 0.11783 and 0.117835 for time period of 6.0×10^3 with $\delta t = 0.03$.

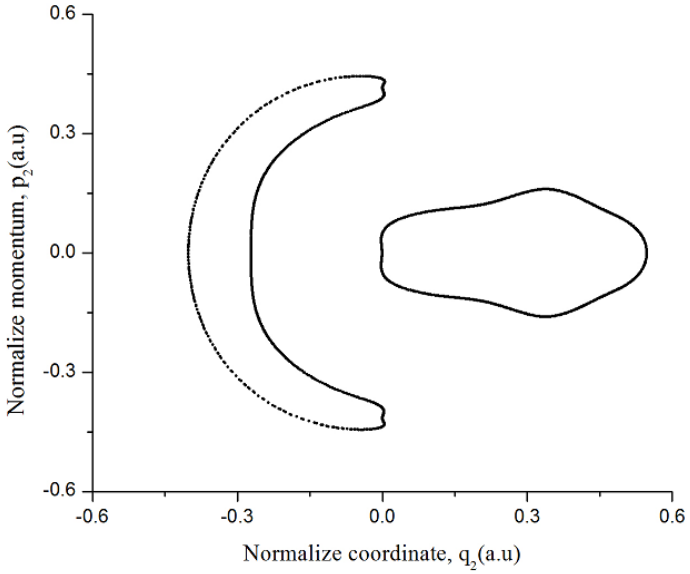

(a)

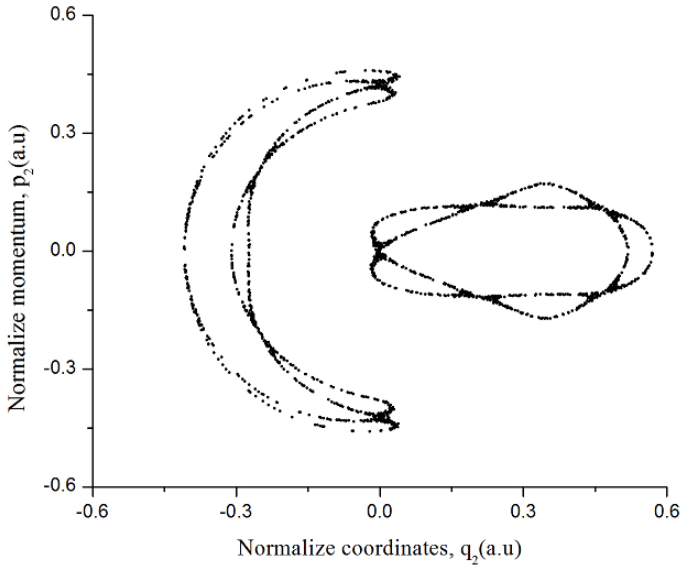

(b)

Figure 3.5: *Plots of Henon-Helies system by using SIA with initial conditions of* $(q_1, q_2, p_2)_{initial} = (0, 0, 0)$, $(p_1)_{initial} = \sqrt{2H}$. *For (a) H= 0.11783 and (b) H= 0.117835.*

To summarize this section we can say that SIA is very sensitive, greatly depends on the initial conditions and total energy, while RKA shows no such dependencies. Hence in the next chapter we have used SIA to find the exact trajectories of passing and trapped particles in tokamak magnetic field.

Chapter 4

Trajectory calculation of fast ions in tokamak using SIA

The main objective of this chapter is to calculate the trajectories of fast ions (alpha particles) in tokamak plasmas in the presence of magnetic field perturbation. The simulations are carried out for circular flux surfaces. We have investigated for trapped and passing particles, how trajectories depend on energy and on toroidal field ripples. The resonance between toroidal precession of bananas and the toroidal field ripples have been highlighted.

4.1 Model for steady-state magnetic field perturbations

High temperature plasma of about $10KeV$ is required to achieve fusion reactions. To heat the plasma to such temperature is a very big issue. Hence several techniques are used to heat plasma to some specific temperature and thus to attain desirable conditions for fusion. The mechanism of key interest here is self-heating process or internal-heating process: in which fusion products like fast alpha particles transfer most of their birth energy to plasma species through collisions. In fusion perspective fast ions are almost impossible to ignore, therefore in this portion we are going to study the behaviors of fast ions in tokamak in the presence of steady magnetic perturbations like TF ripples. SIA technique is used to study the trajectories of fast ions having much higher energies than plasmas species while considering approximation like circular flux surfaces magnetic configurations, large aspect ratio and plasma pressure is

comparatively low [31, 32]. Hamiltonian of fast alphas is

$$H(\mathbf{p},\mathbf{q}) = \left[\frac{b(p_1,\mathbf{q})}{g}\left\{\psi(\mathbf{p}) + p_2\right\}\right]^2 + \mu b(p_1,\mathbf{q}). \tag{4.1}$$

Here g and all other terms have their usual meaning as discussed in Ch 2. In the presence of perturbations like TF ripples the normalized field strength b can be written as the superposition

$$b(p_1,\mathbf{q}) = b_{as}(p_1,q_1) + b_{TFR}(p_1,\mathbf{q}), \tag{4.2}$$

where b_{TFR} describes the TF ripples strength and b_{as} represent the strength of non perturb axi-symmetric field.

4.1.1 Model for safety factor q_s and poloidal flux ψ

Radial dependence of the safety factor q_s used in our code is of the form

$$q_s(r) = \frac{q_{s0}}{1+\frac{cr^2}{a^2}}, \tag{4.3}$$

where

$$c = \frac{q_{s0}}{q_{sa}} - 1\ . \tag{4.4}$$

Here safety factor at the magnetic axis and safety factor at plasma boundary are denoted by q_{s0} and q_{sa} respectively. The expression used to calculate poloidal flux ψ is [24]

$$\psi = \int_0^r \frac{r\acute{}d r\acute{}}{q_s(\hat{r})} \tag{4.5}$$

The radial profiles of the modelled safety factor and of the poloidal magnetic flux are shown in the Fig. 4.1.

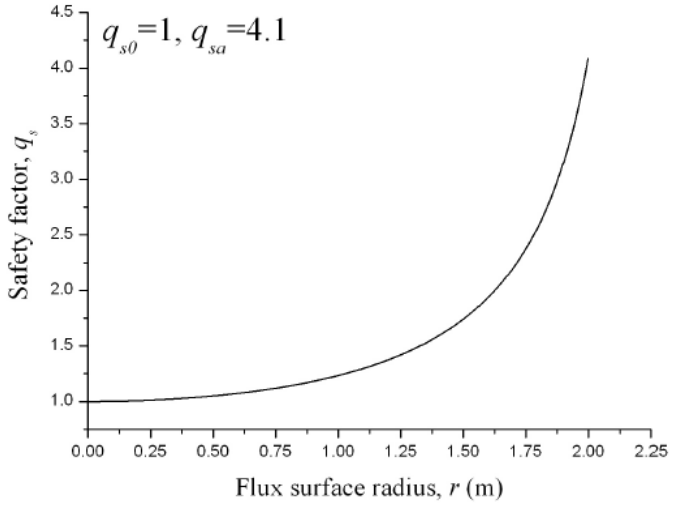

(a)

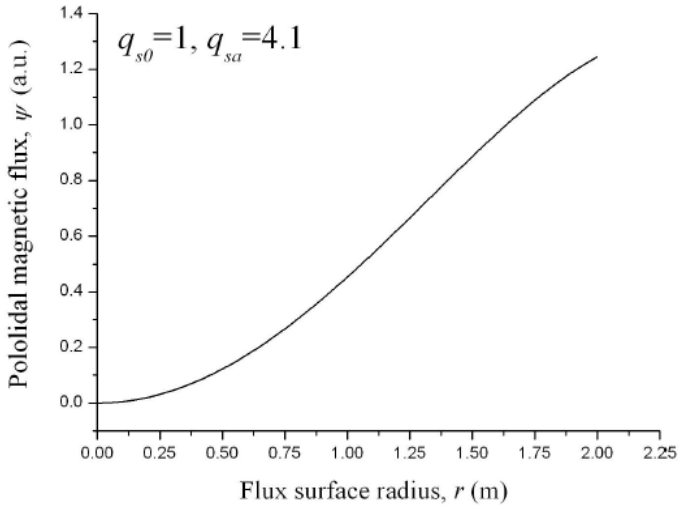

(b)

Figure 4.1: *Radial dependence of (a) safety factor q_s (b) poloidal flux ψ*

4.1.2 Model for TF ripples perturbation b_{TFR}

Describing our model the magnetic perturbation corresponds to TF ripples is taken as

$$b_{TFR} = \delta_{TFR} \cos(N q_2) \tag{4.6}$$

In last equation amplitude of TF ripples is denoted by δ_{TFR} and number of toroidal field coils is given by N. The expression of TF ripples amplitude is [21, 33]

$$\delta_{TFR} = \delta_{TF0} I_0(F), \tag{4.7}$$

where the parameter δ_{TF0} indicates the minimum ripples amplitude, while I_0 is the modified Bessel function with the argument [34, 35]

$$F = N \sqrt{\frac{(R_r - R)^2 + Z^2}{R_r R}} \ . \tag{4.8}$$

Here R_r gives the radial position in the mid-plane where δ_{TFR} reached to its minimum value, i.e. δ_{TF0} as shown in the Fig. 4.2.

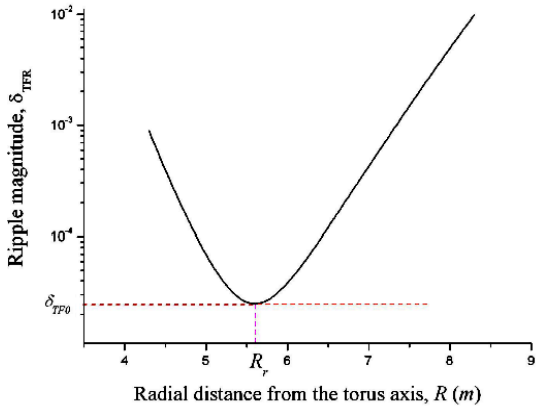

Figure 4.2: *Radial dependence of modelled ripples amplitude* δ_{TFR}.

The above Fig. clearly indicates δ_{TFR} and its radial dependence. It is shown that at the outer edge of tokamak value of δ_{TFR} is 10 times higher than at the inner edge. Cylindrical coordinates used in Eq. (4.8) is

$$R = R_0 + r\cos q_1 \tag{4.9}$$

and

$$Z = r\sin q_1 \tag{4.10}$$

The parameters like $R_r = 5.6$, $R_0 = 6.3$ and $\delta_{TF0} = 2.5 \times 10^{-5}$ are assign here to calculate TR ripples field in a tokamak having size as that of ITER.

Figure 4.3 show variation of b_{TFR} with flux surface radius r. It is clear that up to some specific value of r no change occur in b_{TFR} but after exceeding critical value an exponential increase occur in b_{TFR}.

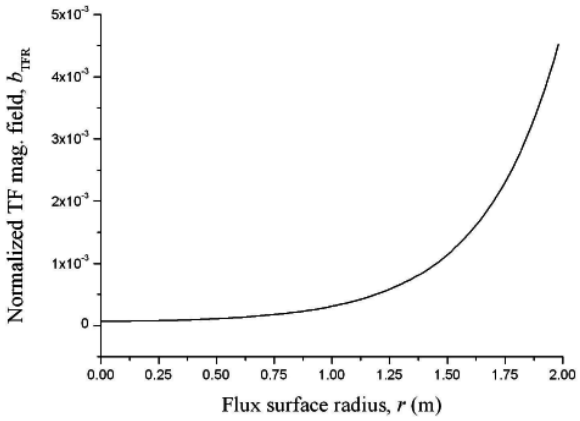

Figure 4.3: *Radial dependence of the modelled ripple strength in the mid-plane for ITER size parameters*

4.1.3 Super banana orbits and ripples resonances

Toroidal magnetic field, $\mathbf{B}_T$, is produced by the result of poloidal winding on torus, on the inner side of the torus the winding is very close to each so the magnetic field is strong on the inner side while on the outer side of the torus the winding is away from each other so magnetic field is weaker in the outer side therefore the magnetic field of tokamak is non homogenous which results in the trapping of some particles which move back and forth between the region

of stronger magnetic fields. If these bouncing particles are subjected to TF ripples it results in considerable increase the radial diffusion coefficient.

When the toroidal distance between two consecutive, lower or upper banana, tips is a multiple of the toroidal separation between adjacent TF coils, the particle bounce motion is said to be in resonance with the toriodicity of TF ripples. If this condition is satisfied resonance phenomena act in to play and can increase the process of fast ions loss from the trapped region. These resonances between the toroidal precession of banana orbits and the TF ripple periodicity bring about a banana guiding center motion and tracing out a so-called superbanana orbit with a new type of radial excursions [21, 36].

After one bounce period if $d\phi = \phi_{i+1} - \phi_i$ is the toroidal angle shift between two consecutive lower banana tips, then the resonance condition is

$$d\phi = l \times \textit{(toroidal distance between adjacent TF coils)} \tag{4.11}$$

$$d\phi = l\frac{2\pi}{N}, \tag{4.12}$$

Dividing Eq. (4.12) by τ_b (bounce time period), we find

$$N\frac{d\phi}{\tau_b} = l\frac{2\pi}{\tau_b} \tag{4.13}$$

or,

$$N\omega_t = l\omega_b, \tag{4.14}$$

where $\omega_t = d\phi/\tau_b$ indicate toroidal precession and $\omega_b = 2\pi/\tau_b$ gives the bounce frequency.

4.2 Trajectories of fast alpha particles in tokamak in axi-symmetric B-field

SIA simulation technique is used to study the trajectories of fast alpha particles in tokamak in influence of perturb and non perturb magnetic fields. In this section our interest is to find the

trajectories in non perturb magnetic configuration, i.e. $\delta_{TFR} = 0$ and non homogenous axi-symmetric magnetic field. The supposition here is that tokamak we are dealing is of ITER size parameters (as mention in the above section) and $B_0 = 5T$, $q_{sa} = 4.1$ and $q_{s0} = 1$. Fast alpha particles moving in the tokamak with birth energies in the range of $0.25\text{MeV} \leqslant E \leqslant 6.8\text{MeV}$ are calculated. Some trajectories of fast alphas are shown in the Fig. 4.3.

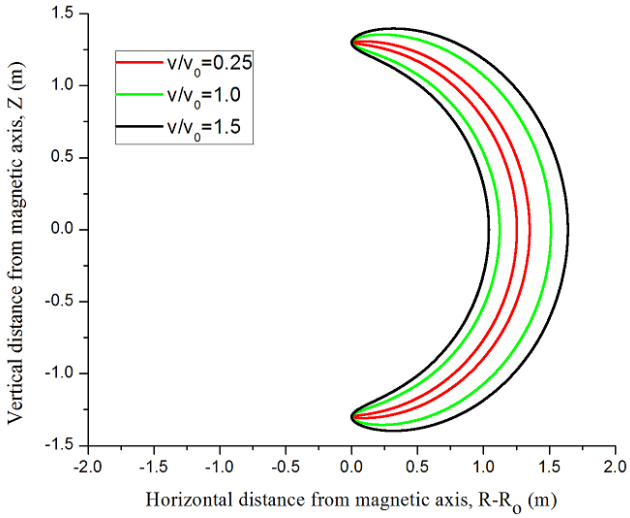

(a)

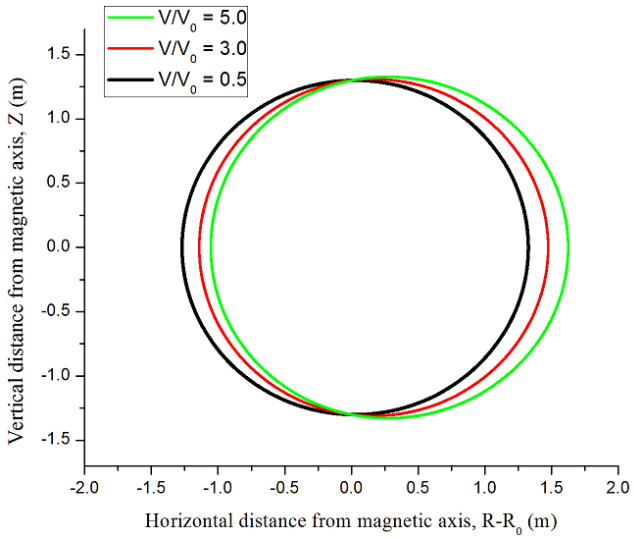

(b)

Figure 4.4: *Projection of (a) trapped alpha particles orbits and (b) passing alpha particles orbits; on to the poloidal plane for an axi-symmetric magnetic field for differernt starting speeds.* R-$R_0 = 0$, *Z=-1.3,* $q_2 = 0$ *and* $v_{\|} = 0$ *defines starting point of each trajectory.*

Figure 4.4a shows poloidal projection of the guiding center orbits of toroidally trapped fast alphas having the same starting positions $R(0)$, $Z(0)$, $p_2(0)$ and $q_2(0)$ and different speeds, $V_0 = 1.3 \times 10^7 m/s$ is taken as a reference speed of alpha particles with birth energy of $E =$ 3.52MeV. As speed of alphas increases the banana width also increases, i.e. For higher V wider will be banana orbit and vice versa, i.e. high energy ions have wider banana orbits. So from this discussion the consequence is very clear that banana width is directly preoperational to energy of alpha particle. Relation of banana width and V is as follow [4]

$$\delta_{Ba} \propto \frac{mv}{q\mathbf{B}_\theta} \tag{4.15}$$

where δ_{Ba} denotes width of banana orbit, $\mathbf{B}_\theta$ poloidal magnetic field, m mass of alpha particles, V velocity of alpha particles and $\in = r/R$ is inverse aspect ratio.

Equation (4.15) explain that width of banana orbit increase by increasing V or alpha particles energy. One must remember that alpha particles with wide banana orbit can easily to escape from the trapped region and become untrapped as compared to those particles whose banana orbits are narrow.

In Fig 4.4b trajectories of passing (untrapped) alpha particles are shown for different alpha speeds. For passing particles an orbit shift phenomena occur by changing velocity or energy of particles. Greater orbit shift occur for passing particle with high speed or high energy while small orbit shift results for particles having low speed or low energy. Orbit shift relation is [4]

$$\delta_P = \frac{mv}{q\mathbf{B}_\theta} \in \quad = \rho_{L\theta} \in, \tag{4.16}$$

where δ_P indicate orbit shift of passing particles in tokamak.

Conservation with relatively accuracy of order of 10^{-10} of energy and toroidal momentum for long term simulation by using SIA are shown in the Fig. 4.5.

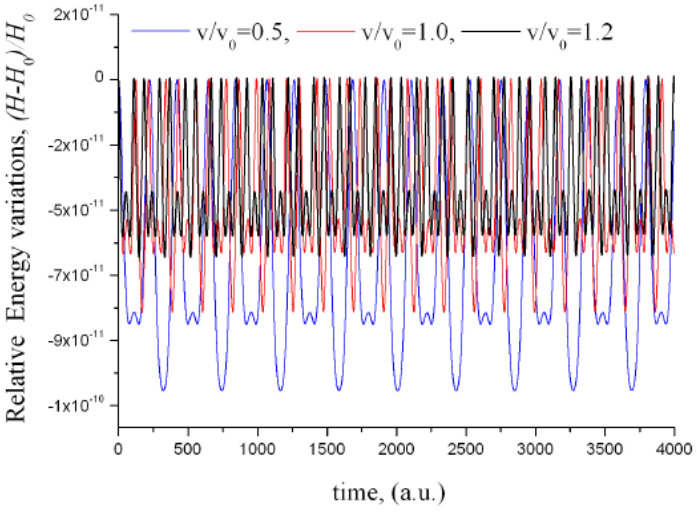

(a)

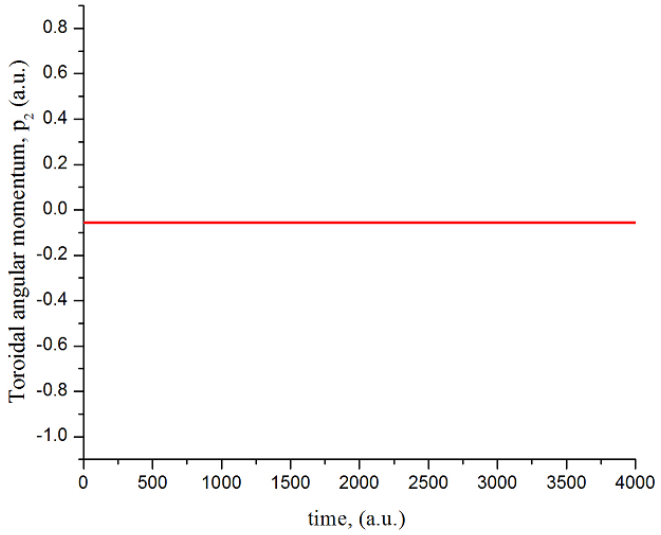

(b)

Figure 4.5: *For long time simulation, conservation of (a) total energy (b) toroidal angular momentum.*

In the absence of TF ripples no dispersion occur in the banana orbit tips and therefore the alpha particles are well trapped in this case as depicted in the zoomed banana tip for several bounce periods in Fig. 4.6.

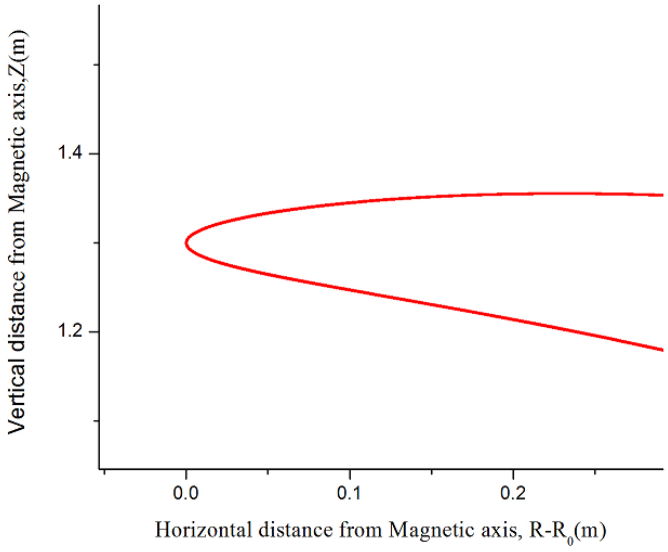

Figure 4.6: *Zoom tip of banana orbit in the absence of TF ripples*

A 3D plot shown in Fig.4.7 shows the motion of trapped alpha particles with birth energies of 3.5MeV in a non perturb magnetic configuration.

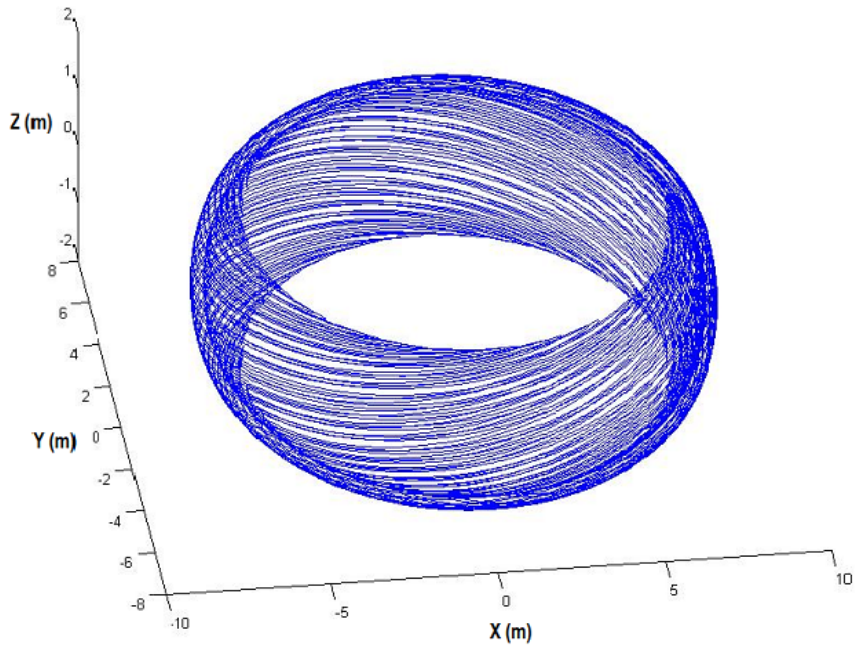

Figure 4.7: *3D orbit of a 3.5 MeV alpha particle toroidally trapped in an axi-symmetric magnetic field. Trajectories starting points are ($R_{0,}$ 0, -1.3m) and $V_{\|} = 0$*

4.3 Alphas trajectories in the presence of TF-ripples

Trajectories of fast alpha particles are shown in the Fig. 4.6 under the influence of magnetic perturbation namely TF-ripples in tokamak configuration. TF-ripples amplitude are taken here as $\delta_{TFR}^{\max} = 1\%$. For three resonance levels l, the orbit excursion over few bounce periods as induced by ripple resonance are highlighted in the plots.

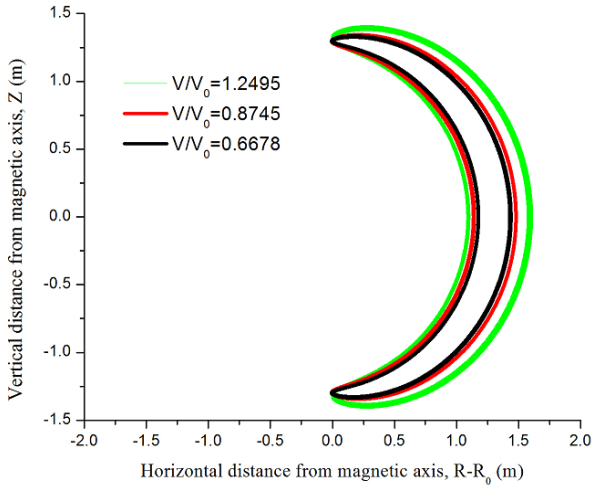

(a)

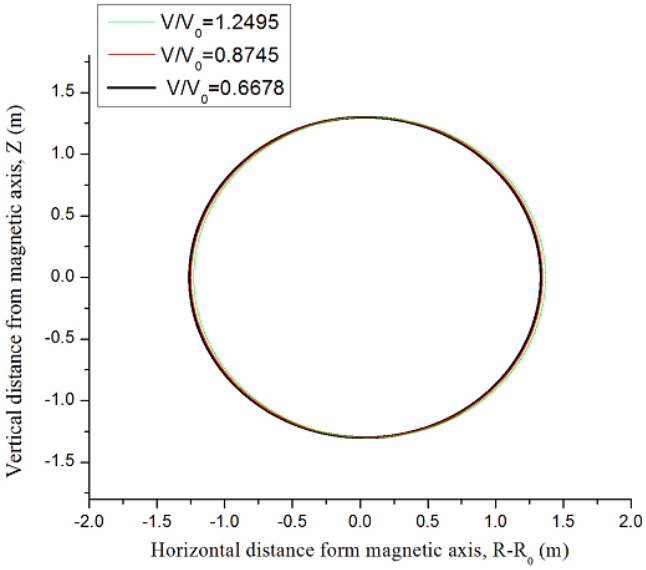

(b)

Figure 4.8: *Projection of (a) trapped alpha particles orbits and (b) passing alpha particles orbits; on to the poloidal plane in the presence of TF-ripples for different starting speeds. R-$R_0 = 0$, Z=-1.3, $q_2 = 0$ and $V_{\|} = 0$ defines starting point of each trajectory.*

Zoomed tip region of banana orbit in the presence of TF-ripples are shown in the Fig.4.9

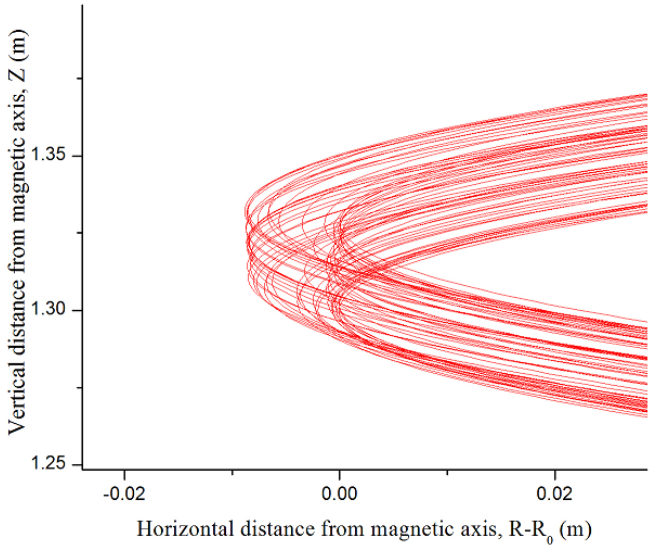

Figure 4.9: *Zoomed tip of banana orbit*

This Fig. indicate that in the presence of TF-ripples the banana orbit tip is much dispersed which in term give the idea that the alpha particles which satisfy ripple resonance condition of Eq. (4.14) cause banana resonance, due to which for some radial displacement of whole banana the super banana motion has been established. Due to resonance it is much easy for fast alphas to get free from the trapped region (to become untrapped), alpha particles losses form the trapped region is very productive specially in the case when the particles are in the tips at the instant when it bounce back, which is not good for tokamak because it produce problems like reduce strength of plasma heating efficiency and heat load concentration.

Figure 4.10 shows that toroidal angular momentum p_2 is no longer conserve in the presence of TF ripples. This non conservation of angular momentum results in the radial diffusion of alpha particles [37].

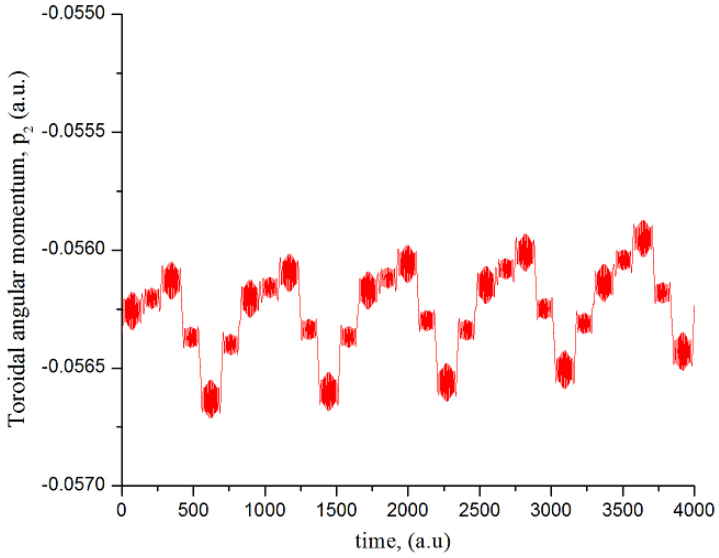

Figure 4.10: *Toroidal angular momentum p_2 in the presence of TF-ripples*

4.4 Conclusion

In this work we use two numerical integration techniques namely Symplectic Integration Algorithm (SIA) and a non symplectic method like Range-Kutta Algorithm (RKA) to describe the numerical integration of Hamiltonian dynamical system like Henon-Heiles Hamiltonian presented by Henon and Heiles and use to describe the motion of stars about its galactic center.

Each time Poincaré maps of star trajectories were plot by using same initial conditions, same period of time, same number of integration steps and the total energy H is also same, for such situation it is concluded that in each case Poincaré maps of star trajectories which results from SIA is very clear, well defined and having knife edge sharp boundaries, no dispersion is there, while in case of RKA Poincaré maps of star trajectories are not well defined, blurred, cloudy, much dispersion is present in its boundaries. The main fact behind this difference is that in case of SIA energy and momentum is conserved, no such big change occur in momentum and energy after each integration step or very small error is collected after each integration step while in case of RKA energy and momentum are not conserved so as result error after each integration step grows. From this discussion we came across the result that for long time

simulation SIA is the best one to implement. Keeping all these behaviors in mind we use SIA to find the trajectories of fast in tokamak.

High energetic alpha particles, i.e. ^4He produce from fusion reactions is used in tokamak to heat plasma up to ignition temperature. The alpha particles born in fusion reactions having birth energy of $3.5MeV$ transfer most of their energy to plasma species through collisions mean fast energetic alpha particles produced self heating phenomena, therefore we can ignore the importance of these alpha particles in tokamak plasmas. The most important is that how these fast alpha particles behaves in perturb and non perturb tokamak magnetic configuration, as well as to find the diffusion rate and factors which effects it. All these needs exact knowledge of particles trajectories. So SIA is used to find the trajectories of fast ions in tokamaks, in the presence of perturb and non-perturb magnetic configuration.

In case of non perturb magnetic configuration trajectories of fast alphas for different velocties were traced out and it is concluded that in case of trapped particles trajectories, width of banana orbit increases with the increase of alpha particle velocity while in case of passing particles orbit shift also increases with increase of alpha particle velocity. Same is the case in the presence of perturbations like TF-ripples, due to TF-ripples also spreading occur in the tips of trapped particle trajectories (banana orbit), which demonstrate that in case of TF-ripples it is easy for trapped particles to escape from trapped region specially on the instant when it bounce back because at that point the effect of TF-ripples is very frequent. Diffusion of fast alphas from the trapped region is not good for the tokamak because such loss reduce alpha particles heating efficiency as well it lead to excessive heat loading and damage to plasma facing components like first wall and divertor plate structure.

Bibliography

[1] J. E. Boom et al., *2D ECE-imaging measurements of edge localised modes (elms) at ASDEX upgrade*, 37th EPS Conference on Plasma Physics, **P2.119** (2010).

[2] I. G. J. Classen et al., *Effect of heating on the suppression of tearing modes in tokamaks*, Phys. Rev.Lett. **98,** 035001(2007) .

[3] L. C. Woods, *Theory of tokamak transport*, Wiley-VCH Verlag GmbH (2006).

[4] J. Wesson, *Tokamaks*, Oxford Science Publication, 3rd edition (2004).

[5] W. W. Heidbrink and G. J. Sadler, *The behavior of fast ions in tokamak experiments*, Nucl. Fusion **34**, 535 (1994).

[6] S. J. Zweben et al., *Alpha particle physics experiments in TFTR*, Plasma Phys. Contr. Fusion **39**, A275 (1997).

[7] P. J. Channell, *Symplectic integration algorithms*, Los Alamos National Laboratory Rep., At-6:ATN-83-9 (1983).

[8] P. J. Channell and C. Scovel, *Symplectic integration of Hamiltonian systems*, Nonlinearity **3**, 231 (1990).

[9] Hong Qin and Xiaoyin Guan, *Variational symplectic interrator for long-time simulations of the guiding-center motion of charged particles in general magnetic fields*, Phys Rev. Lett. **100**, 035006, (2008).

[10] A.-S. Libert, C. Hubaux and T. Carletti, *Symplectic integration of deviation vectors and chaos determination (2010)*, weblink: http://arxiv.org/abs/1005.5611v2.

[11] M. Khan, K. Schoepf, V. Goloborod'ko, V. Yavorskij, *Symplectic Simulation of Fast Alpha Particle Radial Transport in Tokamaks in the Presence of TF Ripples and a Neoclassical Tearing Mode,* J. Fusion Energy **31**, 547 (2012).

[12] Hong Qin, Xiaoyin Guan and William M. Tang, *Variational symplectic algorithm for guiding center dynamics and its application in tokamak geometry*, Phys. Plasmas **16**, 042510 (2009).

[13] S. J. Zweben et al., Alpha-particle physics in the tokamak fusion test reactor DT-experiment, Nucl. Fusion **40**, 91 (2000).

[14] A. Fasoli et al., *Physics of energetic ions*, Nucl. Fusion **47**, S264 (2007).

[15] K. McGuire et al., *Study of high-beta magnetohydrodynamic modes and fast-ion losses in PDX*, Phys. Rev. Lett. **50**, 891 (1983).

[16] S. J. Zweben et al., *MHD induced alpha particle loss in TFTR*, Nucl. Fusion **39**, 1097 (1999).

[17] E. M. Carolipio,W.W. Heidbrink, C. B. Forest and R. B. White, *Simulations of beam ion transport during tearing modes in the DIII-D tokamak*, Nucl. Fusion **42**, 853 (2002).

[18] E. Strumberger, S. Günter, E. Schwarz and C. Tichmann, *Fast particle losses due to NTMs and magnetic field ripple*, New Journal of Phys. **10**, 023017 (2008).

[19] H. H. Duong et al., *The effect of toroidal field ripple on confined alphas in TFTR DT plasmas*, Nucl. Fusion **37**, 271 (2002).

[20] K. Tobita et al., *Ripple-trapped loss of neutral-beam-injected fast ions in JT-60U*, Phys. Rev. Lett. **69**, 3060 (1992).

[21] V. A. Yavorskij, J. W. Edenstrasser, V. Ya. Goloborod'ko, S. N. Reznik and S. J. Zweben, *Fokker-Planck modelling of delayed loss of charged fusion products in TFTR*, Nucl. Fusion **38**, 1565 (1998).

[22] A. I. Morozov and L. S. Solov'ev, *Motion of charged particles in electromagnetic fields*, Reviews of Plasma Phys. (Consultants Bureau, New York) 2, 201 (1966).

[23] F.F. Chen, *Introduction to Plasma Physics and Controlled Fusion*, 2nd ed., Vol. 1: (Plenum Press, New York, 1984).

[24] R. B. White, *The theory of toroidally confined plasmas*, Imperial College Press, England (2001).

[25] R. G. Littlejohn, *Hamiltonian formulation of guiding center motion*, Phys. Fluids **24**, 1730 (1983).

[26] R. G. Littlejohn, *Variational principles of guiding centre motion*, Journal Plasma Phys. **29**, 111 (1983).

[27] J. R. Cary and A. J. Brizard, *Hamiltonian theory of guiding-center motion*, Rev. Mod. Phys. **81**, 693 (2009).

[28] R. J. Goldston, R. B. White and A. H. Boozer, *Confinement of high-energy trapped particles in tokamaks*, Phys. Rev. Lett. **47**, 647 (1981).

[29] L. D. Landau and E. M. Lifshitz, *Mechanics*, Butterworth-Heinemann, Oxford, 3rd edition (1976).

[30] M. Hénon and C. Heiles, *The applicability of the third integral of motion: some numerical experiments*, J. Astron. **69**, 73 (1964).

[31] R. B. White and M. S. *Chance, Hamiltonian guiding center drift orbit calculation for plasmas of arbitrary cross section*, Phys. Fluids **27**, 2455 (1984).

[32] R. B. White, *Chaos in trapped particle orbits*, Phys. Rev. **E 58**, 1774 (1998).

[33] P. N. Yushmanov, *Generalized ripple-banana transport in a tokamak*, Nucl. Fusion **23**, 1599 (1983).

[34] P. N. Yushmanov, *Confinement of toroidally trapped high-energy particles in a rippled magnetic field*, JETP Lett. **35**, 619 (1982).

[35] V. Ya. Goloborod'ko and Ya. I. Kolesnichenko, *Influence of magnetic field ripples on plasma rotation in tokamaks*, Proc. 10th Int. Conf. on Plasma Phys. Contr. Nucl. Fusion Res. Vol. **2**, 179 (1985).

[36] V. Yavorskij, Zh. N. Andrushchenko, J. W. Edenstrasser and V. Ya Goloborod'ko, *Three-dimensional Fokker-Planck equation for trapped fast ions in a tokamak with weak toroidal field ripples*, Phys. Plasmas **6**, 3853 (1999).

[37] V. Yavorskij, A. Moskvitin, Yu. Moskvitina, V. Goloborodko and K. Schoepf, *3D Fokker-Planck description of TF ripple induced collisional transport of fast ions in tokamaks,* Nucl. Fusion **50**, 084022 (2010).